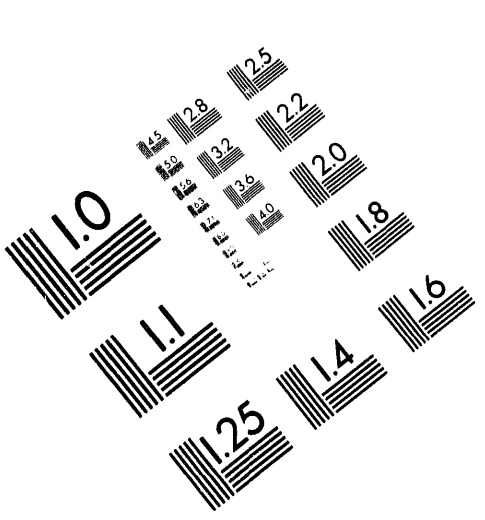

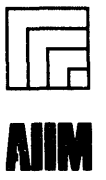

Association for Information and Image Management
1100 Wayne Avenue, Suite 1100
Silver Spring, Maryland 20910
301/587-8202

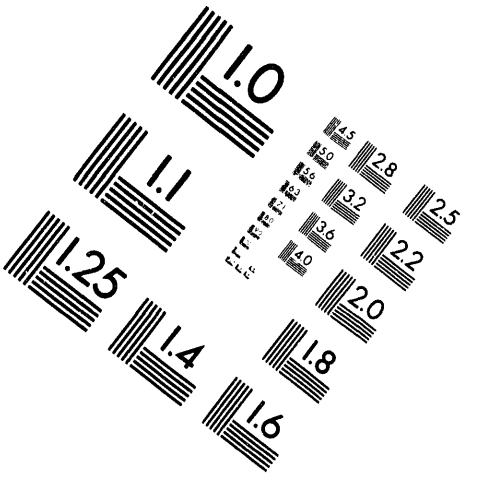

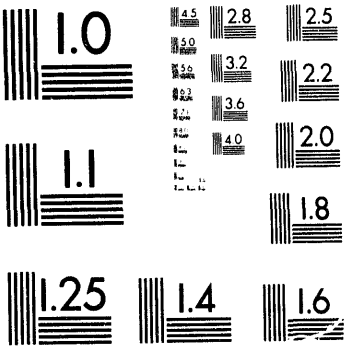

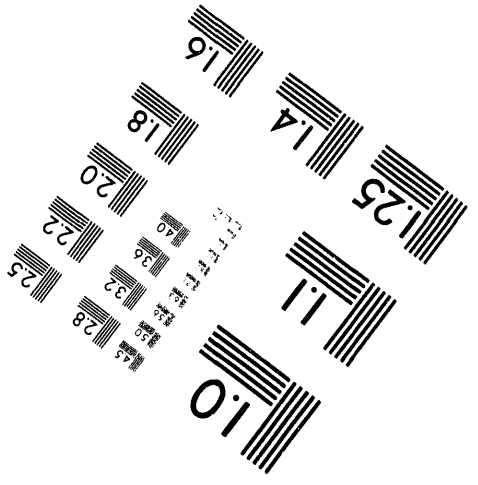

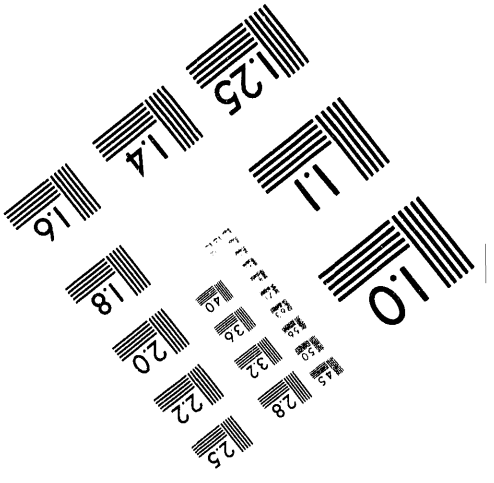

1 of 1

SAND93-4031
Unlimited Release
Printed June 1994

Distribution
Category UC-126

Stability Evaluation of the Markel Mine at Weeks Island, Louisiana

Edward L. Hoffman
Engineering and Structural Mechanics Division
Sandia National Laboratories
Albuquerque, New Mexico 87185

Abstract

A three dimensional (3D) finite element analysis of the Markel Mine located on Weeks Island was performed to: (1) evaluate the stability of the mine and (2) determine the effect of mine failure on the nearby Morton Salt mine and SPR facilities. The first part of the stability evaluation investigates the effect of pillar failure on mine stability. These simulations revealed that tensile stresses and dilatant damage develop in the overlying salt as a result of pillar loss. These tensile stresses extend to the salt/overburden interface only for the case where all 45 of the pillars are assumed to fail. Tensile stresses would likely cause macrofracturing of the salt, resulting in a flow path for groundwater from the overlying aquifer to enter the mine. The dilatant damage bridges between the mine and the overburden in the case where 15 or more pillars are removed from the model. Dilatant damage is attributed to microfracturing or changes in the pore structure of the salt and could also result in a flow path for groundwater to enter the mine.

The second part of the Markel Mine evaluation investigates the stability of the pillars with respect to three failure mechanisms: tensile failure, compressive failure, and creep rupture. A 3D slabbing pillar model of the Markel mine was developed to investigate progressive failure of the pillars and the effect of slabbing on mine stability. Salt was removed from the initially square pillars to form hourglass-shaped pillars similar to the post-spalled shape of the Markel Mine pillars. Prior to slabbing, tensile stresses were predicted in the sidewalls and corners of the pillars in a pattern consistent with the failures observed in the Markel Mine. After slabbing, the pillar stresses redistribute such that there are no tensile stresses in the pillars. It is proposed that the corner slabbing observed in the Markel Mine was caused by the development of tensile stresses in the pillars and that, based on a tensile failure criterion, no further tensile failure is imminent. Vertical stress increases due to the reduction in the pillar area after slabbing are not sufficient to initiate compressive failure. Based on a strain-limiting creep rupture criterion, pillar failure is predicted to be extensive at present. The associated loss of pillar strength should be equivalent to removing all pillars from the model as was done in the first part of this stability analysis, resulting in the possibility of ground water intrusion. Since creep rupture is not a well understood phenomenon, further development and validation of this criterion is recommended.

Contents

Figures

Tables

1 Introduction

The Weeks Island SPR mine is a two-level room and pillar mine acquired from Morton Salt Company in 1976. The 1976 purchase agreement allowed Morton to continue utilizing the existing mine shafts for development of an interim mine, known as the Markel Mine, while two shafts were being sunk for the New Morton Mine. The Markel Mine was active until 1981. Figure 1 shows the relative locations of the SPR mine (labeled "Upper Mine Level" and "Lower Mine Level"), Markel Mine, and New Morton Mine. The Markel Mine is located approximately 305 m (1000 ft) to the northwest of the SPR mine. Furthermore, the service shaft to the New Morton Mine is approximately 152 m (500 ft) south of the Markel Mine.

Since abandonment, the Markel Mine has been periodically inspected for possible signs of instability. The condition of this mine is of concern for two reasons. First, given the close proximity of the underground workings, there is concern that deterioration of the Markel Mine could possibly impact operations of the SPR and Morton facilities. Second, since the Markel Mine is at the same depth and utilizes similar extraction ratios as the upper level of the SPR facility, close monitoring of the condition of the Markel Mine is insightful as to the condition of the SPR facility which is not as accessible. Sandia, in its role of providing geotechnical support for the SPR, is interested in the impact of Markel Mine deterioration on the SPR and the New Morton Mine. The principal concern is the potential for hydrological impact (e.g. leaks) caused by the deterioration of the Markel Mine. The ground water regime

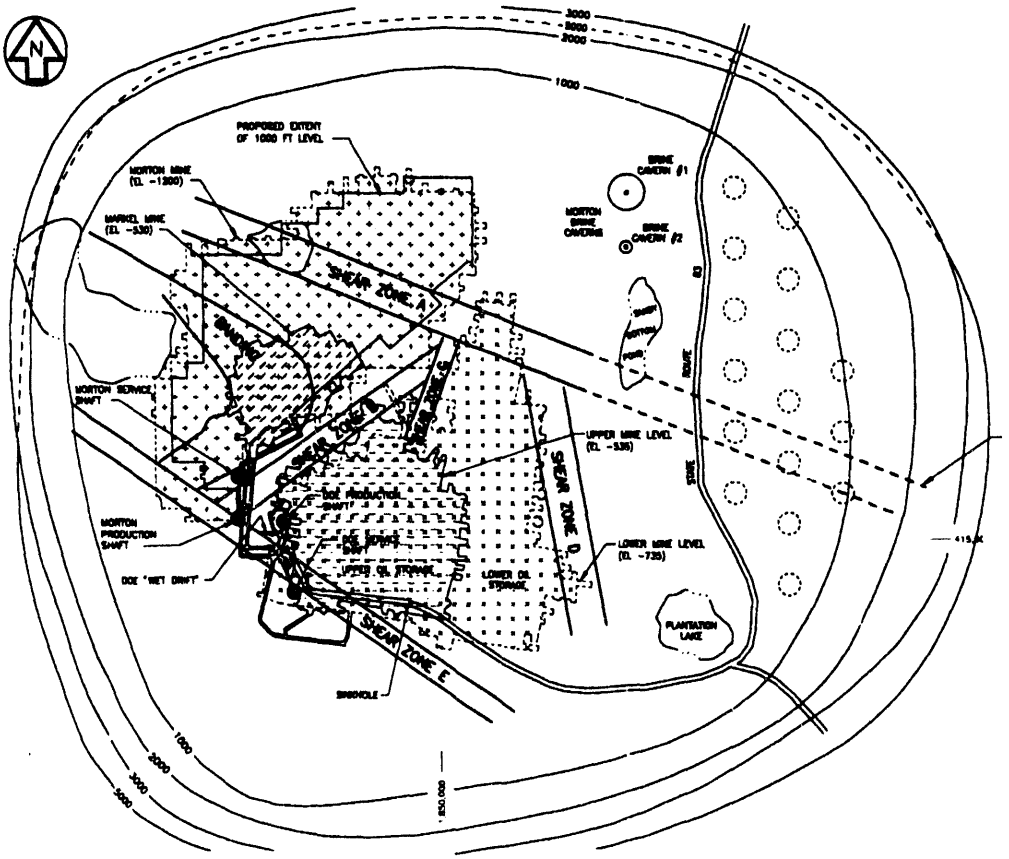

Figure 1. Locations of mines at Weeks Island, including the SPR oil storage facility, the Markel Mine, and the New Morton Mine.

over the Weeks Island dome is a single aquifer which extends from just below the surface (at mean sea level) to the top of the salt stock [1]. The silt and clay above the dome do not provide a ground water barrier above the dome. Hence, the water immediately above the salt is nearly saturated with salt. In the event that a leak developed through the salt into the underground workings, the initial inflow would be saturated. However, later flow would be from the less saline portion of the aquifer, causing the rate of solutioning, and thus leakage rates, to increase. The sudden inflow of fresh water into the mine could result in flooding of the Markel Mine.

Flooding of the Markel Mine could pose a threat to both the Weeks Island SPR oil reserves and the New Morton Mine. The only barrier between the SPR facility and the Markel Mine are isolation bulkheads. The bulkheads, located in each of the two access drifts that connect the mines, are approximately 40 ft-long, keyed into the salt, and are designed to isolate the SPR from a flood. Both the service and production shafts of the New Morton Mine are approximately 18 m (60 ft) from one of the access drifts to the Markel Mine. In the event that the Markel floods, 18 m (60 ft) of salt may not be a sufficient barrier. Any breach of the shaft lining would result in ground water flow towards the Morton Mine. Sufficient recharging of the unsaturated ground water could occur and result in uncontrolled flows into the mines. Finally, the service shaft of the New Morton Mine is located approximately 152 m (500 ft) to the south of the Markel Mine. Surface subsidence resulting from the creep closure of the Markel Mine may cause damage to this service shaft.

In this stability investigation, three-dimensional (3D) finite element models of the Markel Mine are used to evaluate the impact of a Markel Mine collapse on the SPR and Morton facilities. All of the calculations were performed using JAC3D [2]. There are two primary concerns addressed in these calculations: (1) the effect of pillar loss on the stability of the mine and (2) the present condition of the Markel Mine pillars. First, calculations are presented which investigate the effects of pillar failure on mine stability. In this model no mechanism is presented as the cause of failure. Instead, selected pillars are removed from the model using the element death option in JAC3D. The effects of the pillar deletions on the stress distribution surrounding the mine and in the remaining pillars are investigated. Second, a model of the Markel Mine is presented which investigates the effect of progressive failure of pillars on mine stability. Salt was removed from the initially square pillars to form hourglass-shaped pillars similar to the post-failure pillar shapes observed in the Markel Mine. The resulting stress redistribution in the pillars is investigated to determine the effect of pillar slabbing on pillar stability. Combined, the two calculations described in this report present the most complete stability evaluation of the Markel Mine possible considering the current state of technology in modeling salt. Although this study answers many questions and provides valuable insight into the stability of the Markel Mine, some questions remain unanswered. For example, the study identifies a mechanism to which the existing pillar failure can be attributed. Furthermore, the study reveals that the hourglass shape of the pillar improves the short term stability of the pillar. However, the extent of creep rupture experienced by the pillars, if any, is still unclear since the criterion used in this study has not been extensively validated, making it difficult to estimate the life of the Markel Mine.

A thorough discussion of the finite element model, constitutive models and failure criteria are presented in the next section. In Section 3, the results of the two calculations described above are presented and discussed. Finally, the conclusions are presented in the last section.

2 Numerical Model

2.1 Structural Model

A map of the Markel Mine is shown in Figure 2. The mine consists of a region of 27.4 m (90 ft) high rooms called the benched area and a perimeter area of 7.62 m (25 ft) high rooms called the unbenched area. The roof elevations of the benched and unbenched portions of the mine are the same. The pillars are approximately 29 m (95 ft) square and the rooms are 22.9 m (75 ft) wide in both the benched and unbenched areas, resulting in an extraction ratio of 0.69. The extraction ratio is defined as the room area, measured in a horizontal plane, divided by the total area (including room and pillar). As the figure shows, the mine is somewhat irregular in shape. In the interest of reducing computational costs, a quarter symmetry model approximating the general features of the Markel Mine was developed and is shown in Figure 3. The model geometry simulates a 45 pillar (5 by 9) mine with an unbenched perimeter. Details such as the ramp to the benched area and access drifts are neglected in the model. The model simulates the stratigraphy over the Weeks Island mine which includes a 48.8 m (160 ft) deep sandy overburden layer. Displacements are constrained normal to all four vertical boundaries and the lower horizontal boundary. The model does not include the SPR oil storage facility or the New Morton Mine. Neglecting the SPR site should not have a significant impact on the computational results since, as will be demonstrated later in this paper, the subsidence and stress disturbances of room and pillar mines are localized to a region just outside the mine boundary. However, the effect of neglecting the New Morton Mine is not as insignificant. The mining activities beneath the Markel will cause the floor of

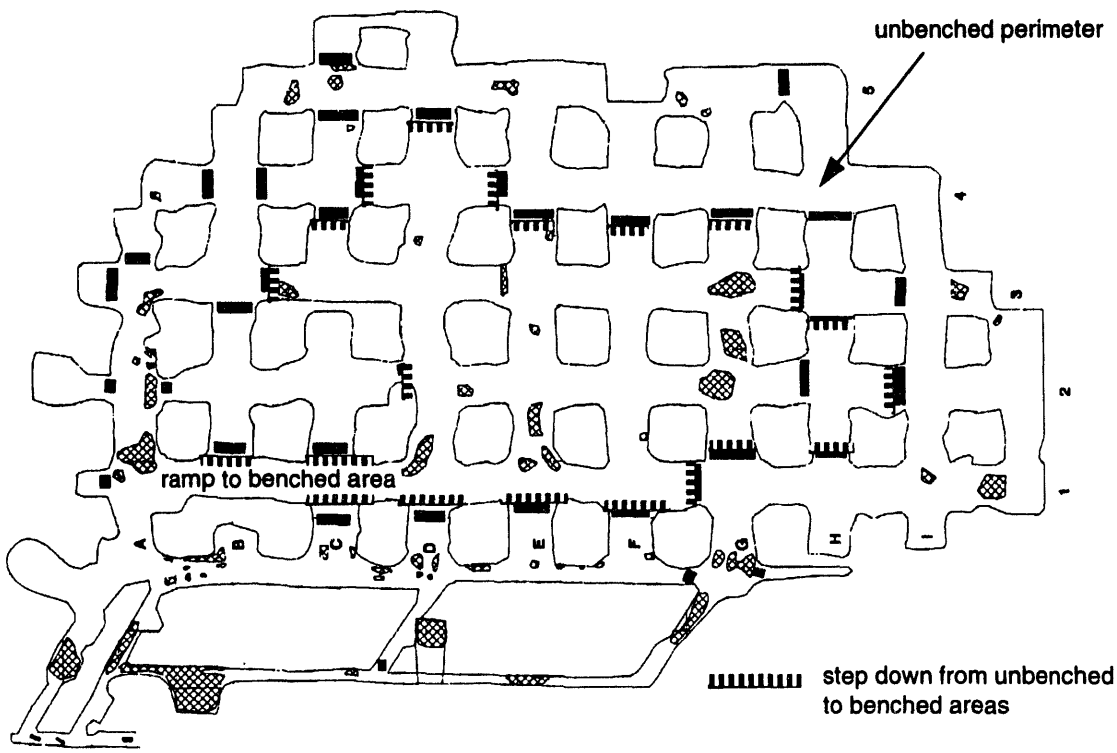

Figure 2. Plan of the Markel Mine.

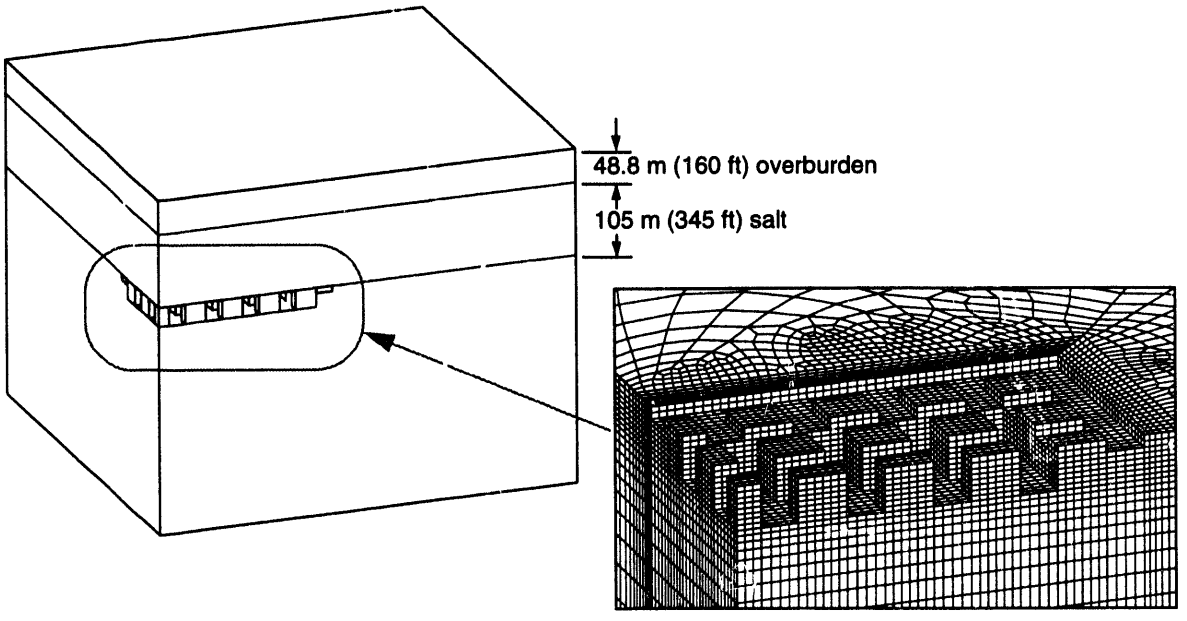

Figure 3. Quarter symmetry model of the Markel Mine, showing the finite element mesh of the mine with the roof removed for clarity.

the Markel to subside, reducing the load on its pillars. However, since this is a stability evaluation of the Markel Mine, neglecting the lower mines has the effect of making the computational results slightly more conservative.

The finite element calculations presented in this memo assume instantaneous formation of the Markel Mine. This may be appropriate as the Markel was mined in a relatively short period (1.5 years). In reality, the 7.62 m (25 ft) high rooms were driven and subsequently enlarged by blasting the bench to form the 27.4 m (90 ft) high rooms. Gravitational body forces are applied to the rock. To ensure initial equilibrium, elevation-dependent initial stresses were applied to each element in the model. The vertical stress component was based on the weight of the overbearing material (using the properties given in Table 1). For the salt, an initial stress state was assumed in which the horizontal stress component is equal to the vertical stress component (lithostatic). For the overburden, the horizontal component was applied to be consistent with a vertically loaded elastic material in equilibrium. Under these load conditions, the resulting ratio of horizontal to vertical stress is defined as follows:

$$\frac{\sigma_h}{\sigma_v} = \frac{\nu}{1-\nu} \tag{1}$$

where ν is the Poisson's ratio of the material.

2.2 Thermal Model

The finite element model includes a depth-dependent temperature gradient which starts at 26.8°C (80°F) at the surface and increases at the rate of 0.0222°C/m (0.012°F/ft). The temperature distribution is important because the creep response of the salt is temperature dependent. One-way thermal coupling was assumed by entering the thermal data into the structural calculations. This assumption was appropriate since the deformations were not large enough to significantly affect the thermal analysis. Furthermore, mine ventilation is assumed to have a minor effect on salt temperature and consequent deformation rates. This assumption is reasonable since it has been demonstrated that cooling effects of oil on storage cavern deformations is negligible [3].

2.3 Material Properties

2.3.1 Constitutive Models

The sandy overburden is modeled as an elastic material, whereas domal salt exhibits both elastic and creep behavior. The creep constitutive model used for this material considers only secondary creep. The creep strain rate depends on the equivalent deviatoric stress as follows:

$$\dot{\varepsilon}^{cr} = A\tilde{\sigma}^{n}\exp\left(-\frac{Q}{RT}\right) \tag{2}$$

where

$\dot{\varepsilon}^{cr}$ is the creep strain rate,

$\tilde{\sigma}$ is the effective or von Mises stress,

T is absolute temperature,

A and n are constants determined from fitting the model to creep data,

Q is the effective activation energy (cal/mole),

R is the universal gas constant (1.987 cal/mole-K).

The properties used for the overburden and salt are reported in Table 1. Although the elastic properties are measured from Weeks Island salt, the creep properties correspond to parameters for the Waste Isolation Pilot Plant (WIPP) salt [4]. Previous studies have shown that WIPP and most SPR salts exhibit similar creep behavior [5, 6].

2.3.2 Structural Stability of Rock Salt

Four failure mechanisms are considered for rock salt in evaluating the stability of the Markel Mine. The first mechanism is *compressive failure* which follows a Mohr-Coulomb yield criterion of increasing strength with increasing confinement pressure. The failure criterion used for this evaluation defines the strength of rock salt in terms of a maximum octahedral shear stress [7] and is based on an extended Drucker-Prager formulation. The equations are presented in Table 2. Although the failure criterion and parameters listed in Table 2 are not specific to Weeks Island salt, they match laboratory data from Weeks Island samples very closely. The parameters given in Table 2 yield an unconfined compressive strength of approximately 19 MPa (2755 psi). Weeks Island Salt has an unconfined compressive strength

Table 1: Structural Properties of Salt and Overburden

Material	Elastic Properties		Density, ρ (kg/m^3)	Creep Properties		
	Young's Modulus, E (GPa)	Poisson's Ratio, ν		A (Pa$^{-4.9}$/sec)	n	Activation Energy, Q (kcal/mole)
Salt	1.28	0.25	2300	5.79×10^{-36}	4.9	12.0
Overburden	0.1	0.33	1874	--	--	--

of 14 to 20 MPa (2030 to 2900 psi) [8]. At a confinement pressure of 3.45 MPa (500 psi) the formulas in Table 2 yield a compressive strength of 35 MPa (5100 psi) whereas tests on Weeks Island salt at this confinement are approximately 34 to 55 MPa (5000 to 8000 psi).

The second mechanism is elastic *tensile failure* or fracturing. It has been the practice in rock mechanics to look for tensile stresses in rock surrounding an underground cavity as a potential source of trouble since rock is not very strong in tension [9]. The measured tensile strength of Weeks Island salt, based on laboratory samples, is approximately 1.07 MPa (155 psi) [8]. For the purposes of these analyses, the tensile strength of Weeks Island salt was assumed to be

Table 2: Equations for the elastic stability limit of rock salt [7]

General Equations:

$\sigma_0 = \frac{1}{3}(\sigma_1 + \sigma_2 + \sigma_3)$	octahedral normal stress
$\tau_0 = \frac{1}{3}\left[(\sigma_1 - \sigma_2)^2 + (\sigma_2 - \sigma_3)^2 + (\sigma_3 - \sigma_1)^2\right]^{1/2}$	octahedral shear stress
$m = \frac{3s_2}{s_1 - s_3}; (s_1 \le s_2 \le s_3)$	Lode parameter
$s_i = \sigma_i - \sigma_0$	stress deviators
$J_m = \frac{m\left(9 - m^2\right)}{\left(3 + m^2\right)^{1.5}}$	invariant of the stress geometry

Equation for the elastic stability limit of rock salt:

$\tau_{0B} = f(\sigma_0)\, g(m)\, h(T)$	stability limit (τ_{0B}) of rock salt
$f(\sigma_0) = b\left(\frac{\sigma_0}{\sigma'}\right)^p$; b=2.7 MPa, p=0.65, σ' =1 MPa	τ_{0B} as a function of octahedral normal stress
$g(m) = \frac{2k}{[(1+k) + (1-k)J_m]}$; k=0.74	stress geometry function
$h(T) = 1$ for $T \le 100$°C	temperature dependence

Equation for elastic stability:

$F_e = \frac{\tau_{0B}}{\tau_0}$	failure is assumed when $F_e < 1$

zero. This assumption is conservative but also may be closer to reality since laboratory tests are based on small samples and large rock samples typically have lower tensile strengths due to inhomogeneities [9]. Tensile cracking in rock salt tends to initiate perpendicular to the largest tensile stress in the rock sample. The largest tensile stress is one of the *principal stresses*. The directions of the principal stresses, called the *principal directions*, are the axes along which the shear stresses vanish. The maximum principal stress is the algebraically largest of the three principal stresses (in 3D space) and the largest normal stress in any direction. The potential for tensile failure exists if the maximum principal stress is tensile. The direction of crack initiation is determined by calculating the corresponding principal direction.

The third failure mechanism is progressive failure due to accumulated creep strain, also known as *creep rupture*. Unlike the previously discussed mechanisms, creep rupture is not instantaneous, but accumulates with time as the salt undergoes creep deformations. Creep rupture is the least understood of the four failure mechanisms considered here for Weeks Island rock salt. The criterion used in this analysis is based on a limiting strain derived from quasistatic laboratory test data [10]. Although the criterion has not been extensively validated against field data, it is the best available measure of the creep rupture performance of Weeks Island salt. The following relationship was derived between the mean stress (pressure, p) and the ultimate strain (ε^u) at failure:

$$\varepsilon^u = a + bp^c \tag{3}$$

where a=1.15, b=1.e-5, and c=1.7614 are material constants. Using this definition of strain-to-rupture, a stability function was defined as follows:

$$F_c = \frac{\varepsilon^u}{\bar{\varepsilon}} \tag{4}$$

where $\bar{\varepsilon}$ is the effective strain. This formulation can be interpreted as a factor of safety in which stability is indicated if $F_c > 1.0$.

2.3.3 Hydrological Performance of Rock Salt

The fourth failure criterion used in the stability evaluation of the Markel Mine relates to the hydrological performance of salt. Rock salt in its natural state is typically considered impermeable. This is why salt formations are considered ideal storage sites for petroleum. The salt above the Weeks Island storage facility isolates the stored oil from the groundwater located above the salt dome. Creep deformations resulting from the excavation of underground openings will not cause an increase in permeability as long as the deformations are isovolumetric. However, deformations that result in an increase in the volume of salt can result in increased permeability. Such a volume increase, called *dilatancy*, is attributed to microfracturing or changes in the pore structure of the salt. The region or volume of salt which experiences a change in its pore structure, or the microstructure of its porosity, due to the excavation of underground openings has become known as the *disturbed rock zone* (DRZ) [11]. Damage in the DRZ is manifested principally as grain boundary microcracking accompanied by dilation, and is a result of relatively high deviatoric and low hydrostatic stresses. *This damage does not imply failure or loss of strength of the rock salt* [11]. Van Sambeek et. al found that the resulting fractures are preferentially aligned parallel to the maximum compressive principal stress and occur almost exclusively on grain boundaries at

the exclusion of cleavage fractures [12]. (In this memo, negative stresses are compressive. Thus, the maximum compressive principal stress corresponds to the algebraically smallest or minimum principal stress.)

Pore structure is the link between mechanical and hydrological response of a porous medium. Pore structure can be altered in two ways: (1) changes can be made to in the existing pore structure, and (2) new pore space can be created. Changes in existing pore structure are made, for example, by changing pressure. An increase in pressure tends to close existing pores and cracks, which reduces the connected porosity and permeability; whereas a decrease in pressure has the opposite effect. Creation of new porosity occurs due to changes in the deviatoric stress state and also increases permeability. The resulting damage increases the hydraulic storage capacity of the rock.

The presence of a DRZ has important implications for the SPR. The increased porosity of the DRZ may serve as a sink within which fluids (oil and water) accumulate. Furthermore, if a DRZ extends from the mine to the groundwater regime just above the salt dome, then a flow path for water into the mine can be established.

Dilatancy surfaces (yield surfaces defined by the onset of volumetric expansion under compressive loading) have been defined in three independent test programs conducted by Hunsche [13], Spiers et al. [14], and Ratigan [15]. A comparison of these three criteria by Sambeek et al. [12] revealed that the dilatancy boundary from any one test, as independently reported, adequately represents the dilatancy boundary for the other tests. This consistency for vastly different salt types provides confidence for applying any one of these criteria. However, there is some variation in the criteria at low mean stress conditions which exist at the shallow depths of the SPR facility at Weeks Island. Dilatation data from Avery Island (a neighboring salt dome of Weeks Island) salt has shown very good agreement with Ratigan's dilatancy surface [15, 16]. This dilatancy surface is defined by a "damage" factor, D, which portrays the potential for dilatant behavior is reported in [12] and is expressed as follows:

$$D = \frac{\sqrt{J_2}}{aI_1} \tag{5}$$

where J_2 is the second invariant of the deviatoric stress tensor, I_1 is the first invariant of the stress tensor ($I_1=3\sigma_m$), and a is a material constant. When D is equal to or greater than one, the shear stresses in the salt are large compared to the mean stress and dilatant behavior is expected.

The criterion, as reported by Ratigan, uses a material constant of a=0.27 to define the slope of the dilatancy surface. Based on quasi-static triaxial compression tests performed on Weeks Island rock salt, Ehgartner [16] demonstrated that Weeks Island salt dilates at lower deviatoric stress than those represented by Ratigan's criterion. Ehgartner determined the constant for this criterion to be a=0.25 for Weeks Island salt. This dilatancy criterion is used in the present study to delineate potential zones of dilatancy in the salt formation surrounding the Markel Mine based on the stress state calculated in the finite element analysis. The orientation of the grain boundary fracture is determined based on the orientation of the minimum principal stress direction (which corresponds to the largest compressive principal stress).

3 Analysis Results

The computational results are presented as two separate investigations. The first and primary investigation is concerned with how the stability of the Markel Mine (including the overlying sand and overburden) is affected by the loss of pillars. Pillar failure is simulated by removing pillars from the model at a specified time using the *element death* option in JAC3D. This method of removing pillars should be an accurate representation of pillar failure since compression tests of salt specimens show a dramatic reduction of strength after failure [17]. Furthermore, it has been demonstrated that the instantaneous removal of pillars yields similar computational results as gradual removal [18]. In this investigation, the two mechanisms of concern are tensile failure and dilatant damage. The development of tensile stresses in the overburden due to the loss of pillars could result in extensive fracturing in the overlying materials and the development of a path for water to enter the mine. Similarly, if a dilatant region or DRZ extends from the mine to the overburden, a flow path for ground water can be established.

The first investigation does not propose how the pillars of the Markel Mine would fail, but only investigates the effect of pillar failure on mine stability. The second investigation examines the stability of the pillars with respect to the three failure mechanisms discussed in Section 2.3 (compressive failure, tensile failure, and creep rupture) in order to evaluate the present condition of the Markel Mine pillars. Progressive failure is modeled by removing salt from initially square pillars to form hourglass-shaped pillars similar to the observed post-slabbed shape of the Markel Mine pillars. This model is used to determine the post-slabbed stress state of the pillars and to evaluate the stability of the pillars after slabbing. Combined, these two investigations present a complete stability evaluation of the Markel Mine considering the current state of technology in modeling salt.

3.1 Finite versus Infinite Room and Pillar Models

The finite room and pillar model of the Markel Mine used in this investigation is intended to be an approximate representation of the irregular geometry of the actual mine. Frequently, infinite room and pillar models are used to represent a mine of finite extent because the models are considerably smaller due to symmetry conditions and are hence less expensive. It is sometimes argued that an infinite model can be an accurate representation of the center pillars of a large mine. To determine whether an infinite model is appropriate for simulations of the Markel Mine, a simulation of an infinite room and pillar model was performed using the same pillar and room dimensions (width, depth, etc.) as the finite model. The infinite room and pillar representation of the Markel Mine is shown in Figure 4. The model represents one-quarter of a pillar and half of the surrounding rooms. Displacements are constrained normal to all four vertical boundaries as well as the lower horizontal boundary. The creep strains in the finite and infinite models are compared in Figure 5 at 10 years into the simulation. The maximum creep strain in the infinite model is 0.1637 but only 0.03744 in the finite model (a factor of 4.4 smaller). Also, the maximum creep strain in the finite room and pillar model occurs in the center pillar, while the pillars closer to the edge experience significantly less creep strain. The shape of the creep strain contours in the infinite model are consistent with those of the finite pillar model, indicating that the deformation mechanisms are similar. The

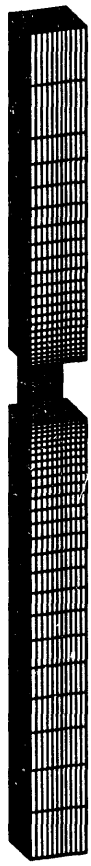

Figure 4. Infinite room and pillar representation of the Markel Mine.

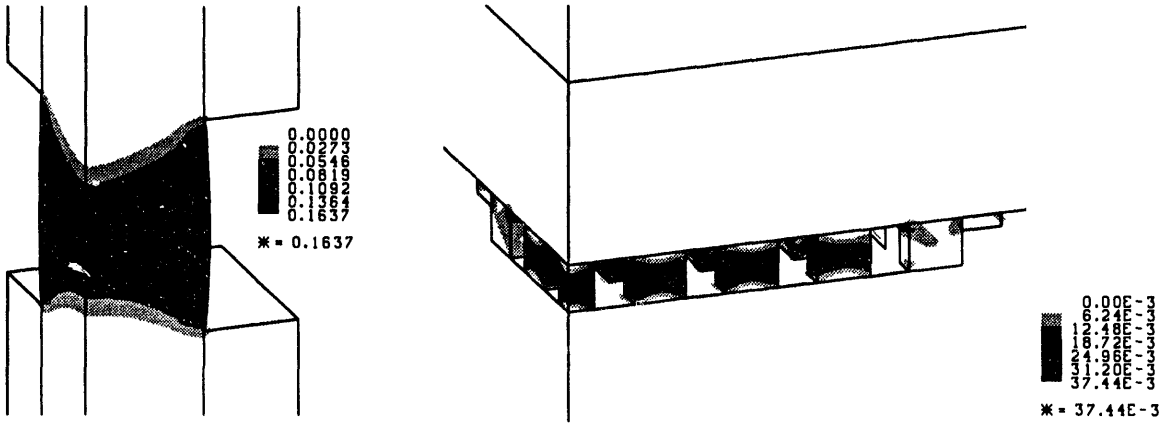

Figure 5. Creep strain at 10 years for infinite and finite room and pillar representations of the Markel Mine (scales intentionally different to show similarity in contour shapes).

maximum subsidence over the infinite room and pillar model is 1.92 m at 10 years into the simulation and only 0.292 m over the finite model (a factor of 6.6 smaller). Thus, the infinite room and pillar model overpredicts both pillar strain and surface subsidence of a 45 pillar mine.

There is a subtle difference between the mechanics of the infinite pillar model and the finite pillar model which is important with respect to evaluating pillar stability. Infinite room and pillar models place the entire weight of the overburden on the pillar, whereas in finite models the surrounding salt bears some of the overburden weight. This is sometimes referred to as *stress arching*. The average vertical stress in the pillar of the infinite model is compared to that of the center pillar of the finite model in Figure 6. Initially, the pillar stress is 10 percent higher in the infinite model. However, this difference becomes greater with time. As the pillars bulge, the load bearing area increases. As a result, the average vertical stress decreases. However, as the pillars shorten in the finite model more load is taken by the material surrounding the mine, resulting in a greater reduction in the pillar stress. This phenomenon is not captured by the infinite room and pillar model. At 10 years into the simulations the vertical stress predicted by the infinite model is 30 percent greater than that predicted with the finite model.

The above comparison is presented to demonstrate the considerations in determining if an infinite room and pillar model is appropriate for a given simulation. The magnitude of the differences between these two models depends on the size of the mine. Since the Markel Mine is a relatively small mine, the differences between these two models are significant. Hence, no

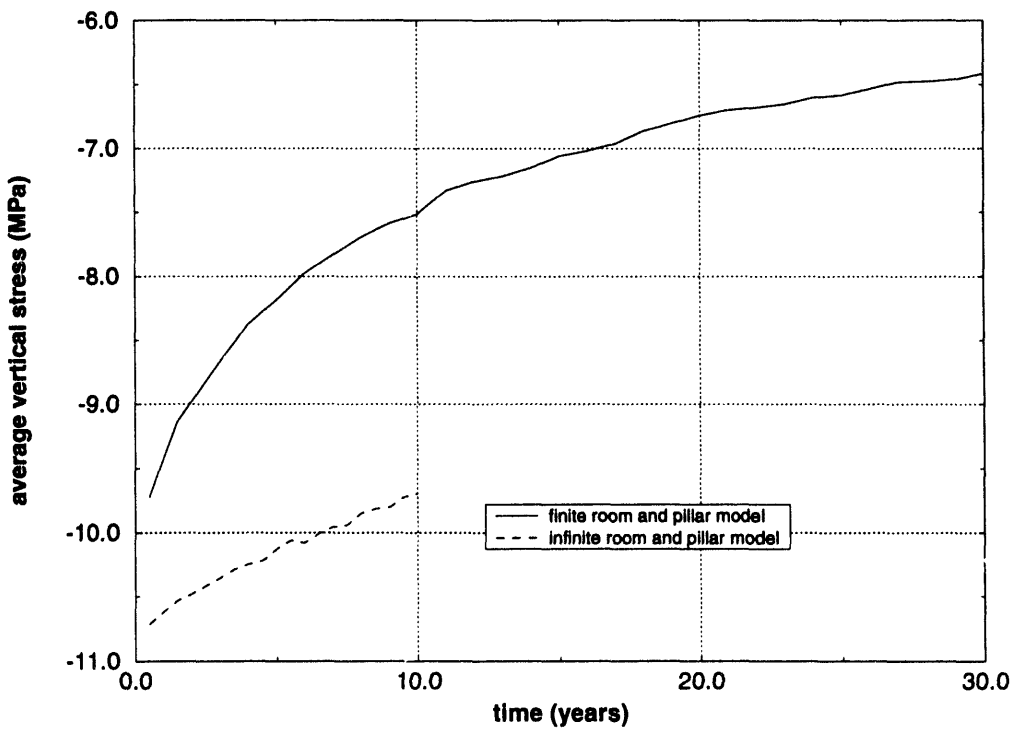

Figure 6. Average vertical stress history in the pillar of the infinite model compared to that in the center pillar of the finite model.

further simulations of the Markel Mine were performed using the infinite room and pillar model.

3.2 Effect of Pillar Failure on Mine Stability

A simulation of the 45 pillar Markel Mine model was performed for 15 years, the approximate age of the mine at present. At this time in the simulation, pillars were removed from the model and the stress redistribution in the overlying strata was evaluated to determine the effect of the pillar loss on mine stability. Five cases were evaluated, simulating the loss of 1, 9, 15, 21, and 45 pillars as illustrated in Figure 7.

3.2.1 Tensile Stress

A contour plot of maximum principal stress is shown in Figure 8 for each of the cases under evaluation. After pillars are removed, a tensile field develops in the roof of the mine. As more pillars are removed the tensile field grows higher and wider. This tensile field reaches the overburden/salt interface only when all 45 pillars are removed. In all of the cases (even when no pillars are removed), a tensile field develops at the surface and extends approximately 213 m (700 ft) from the edge of the mine. The tensile region grows in size and magnitude as pillars are removed from the model. This poses a threat to the service shaft of the New Morton Mine as it is only 152 m (500 ft) away from the Markel Mine. Tensile stress could cause the Morton Mine service shaft to separate from its host salt, creating a flow path behind the shaft lining. A vector plot of the tensile maximum principal stress field is shown in Figure 9 for the case in which all 45 pillars are removed. The tensile stresses are oriented in a vertical direction directly above the mine and gradually transition to a horizontal orientation near the surface. Assuming a tensile strength of zero, cracking would be expected to develop perpendicular to these vectors. As the pillars deteriorate, the high tensile stresses in the roof could cause roof falls.

3.2.2 Dilatant Damage

A contour plot of dilatant damage is shown in Figure 10 for each of the six cases under evaluation. The overburden layer is not shown in this figure as the criterion was developed for rock salt. Damage is indicated where D > 1.0. With no pillars removed the DRZ is confined to a small region surrounding the mine. In the case where 15 or more pillars are removed, the

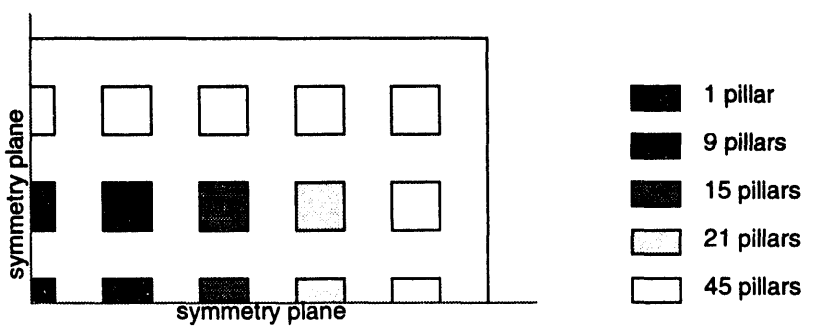

Figure 7. Outline of pillar failure simulations. Each case includes the pillars from the preceding case.

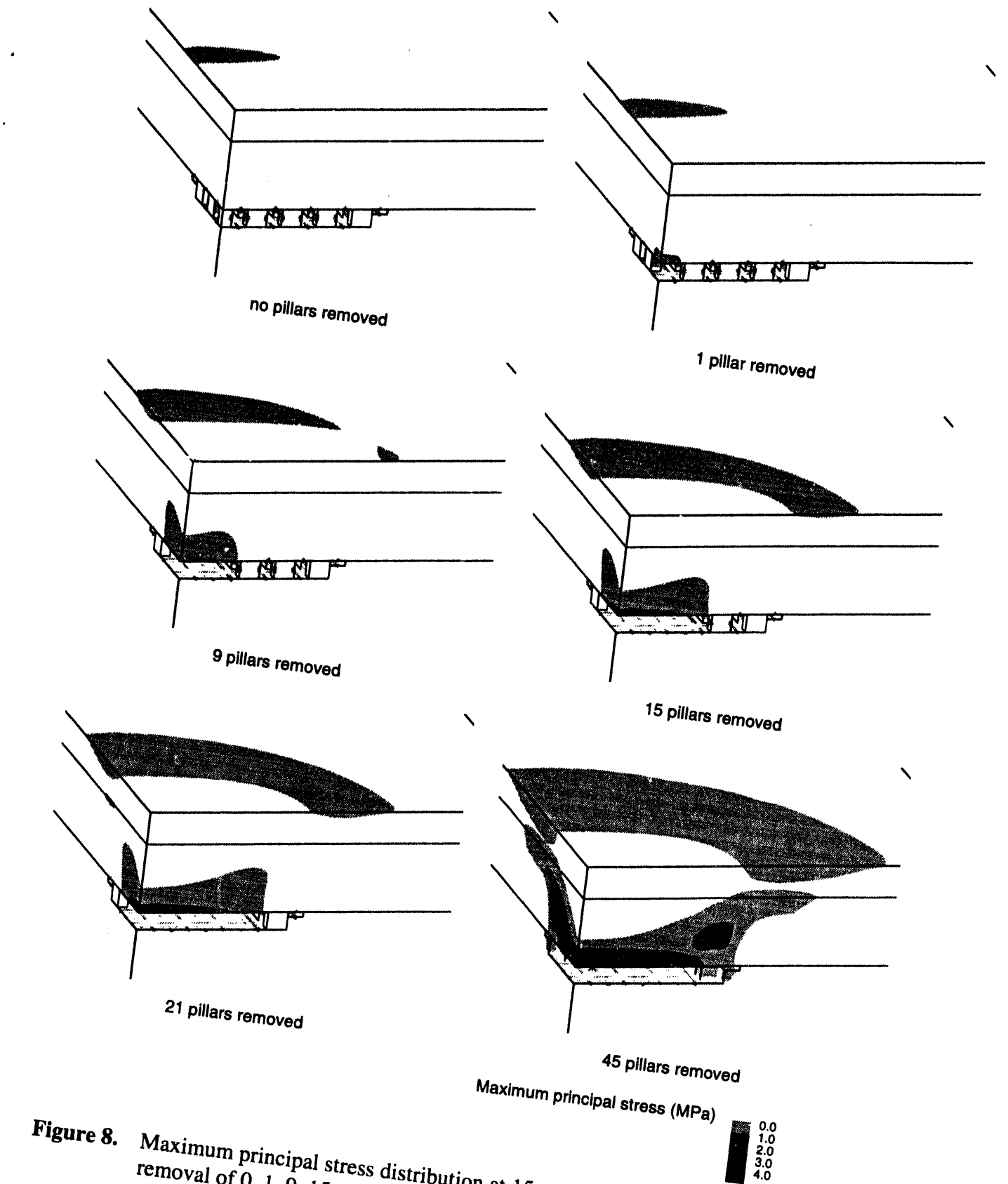

Figure 8. Maximum principal stress distribution at 15 years immediately after the removal of 0, 1, 9, 15, 21, and 45 pillars from the Markel Mine.

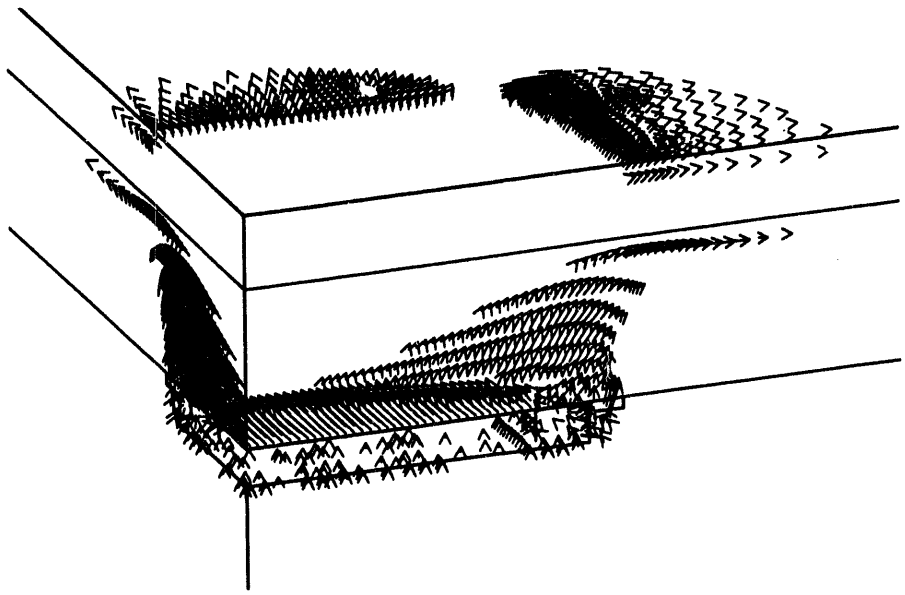

Figure 9. Vector plot of tensile maximum principal stress field in the Markel Mine with all 45 pillars removed.

DRZ bridges between the mine and the overburden/salt interface, creating a flow path for groundwater to enter the mine. As more pillars are removed, the DRZ grows in both size and the magnitude of damage predicted. In the case where all 45 pillars are removed, the damage in the DRZ is predicted to be extensive. The damaged regions correspond to the tensile stress fields presented in the previous section as the tensile stresses reduce the mean stress of the salt.

3.2.3 Stress Redistribution due to Single Pillar Failure

Another item of concern is how the failure of one pillar affects the stress distribution in the surrounding pillars. If the failure of one pillar causes a stress redistribution such that the surrounding pillars fail, then the mine is progressively unstable. Removing the center pillar is a worst case since this pillar is subject to the greatest load. Pillars closer to the mine boundary are subjected to smaller loads due to stress arching effects. Furthermore, when the center pillar is removed the load is redistributed to pillars which are also farther from the mine boundary. The average vertical stress history for one of the off-center pillars is plotted in Figure 11, showing the effect of removing the center pillar. As noted earlier, the average vertical stress decreases in time. The center pillar is removed at 15 years, and the stress in the neighboring pillar increases 8.5 percent. However, this stress is still smaller than the initial vertical stress sustained by the pillar, and much less than the 13.9 MPa unconfined compressive strength of rock salt. Thus, it appears that the loss of only one of the Markel Mine pillars does not significantly affect mine stability.

3.2.4 Surface Subsidence

The influence of pillar loss on surface subsidence is important since subsidence can possibly be used as an indicator of the condition of the mine. Under stable conditions, subsidence is

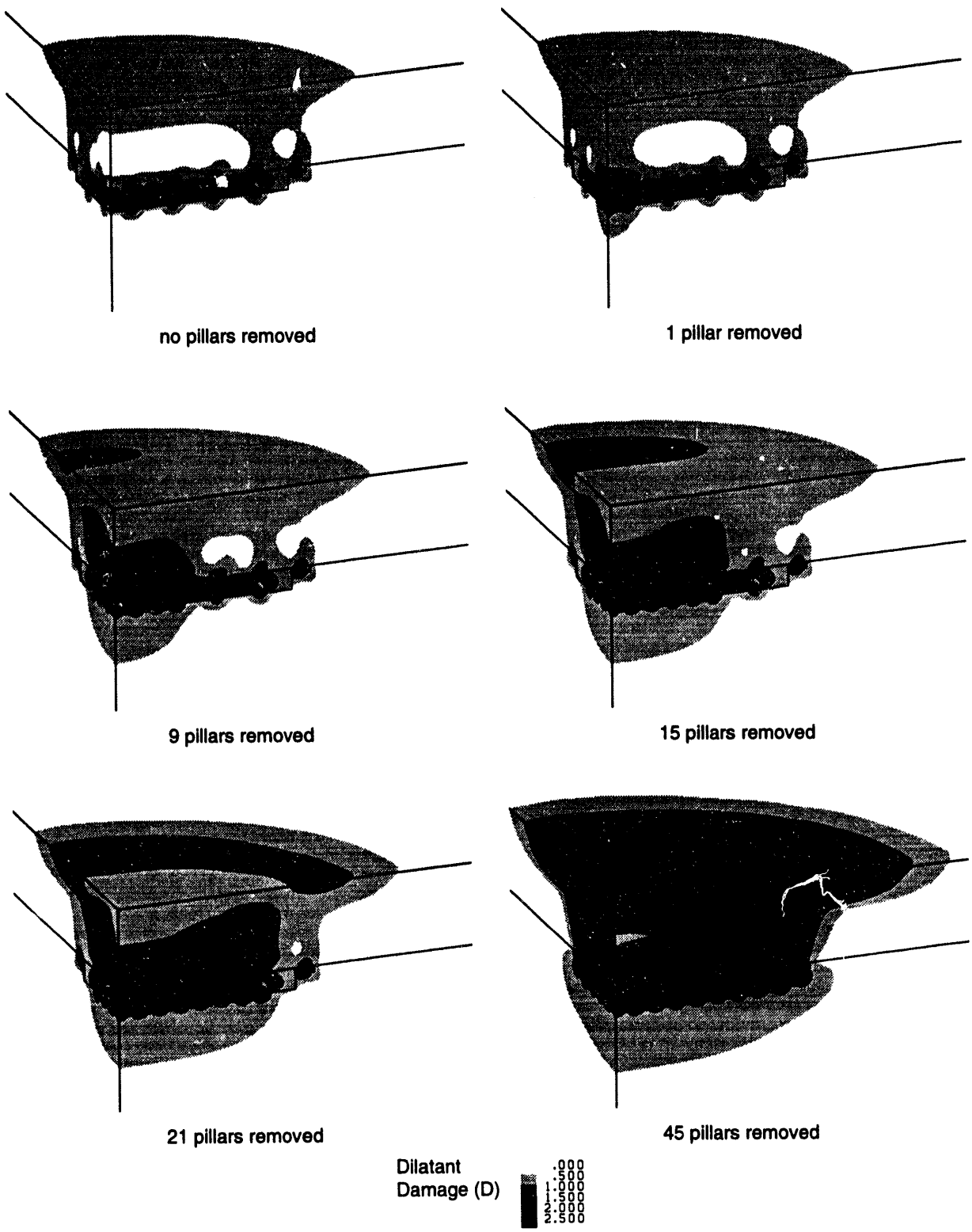

Figure 10. Dilatant damage distribution at 15 years immediately after the removal of 0, 1, 9, 15, 21, and 45 pillars from the Markel Mine. Damage is indicated where $D > 1.0$.

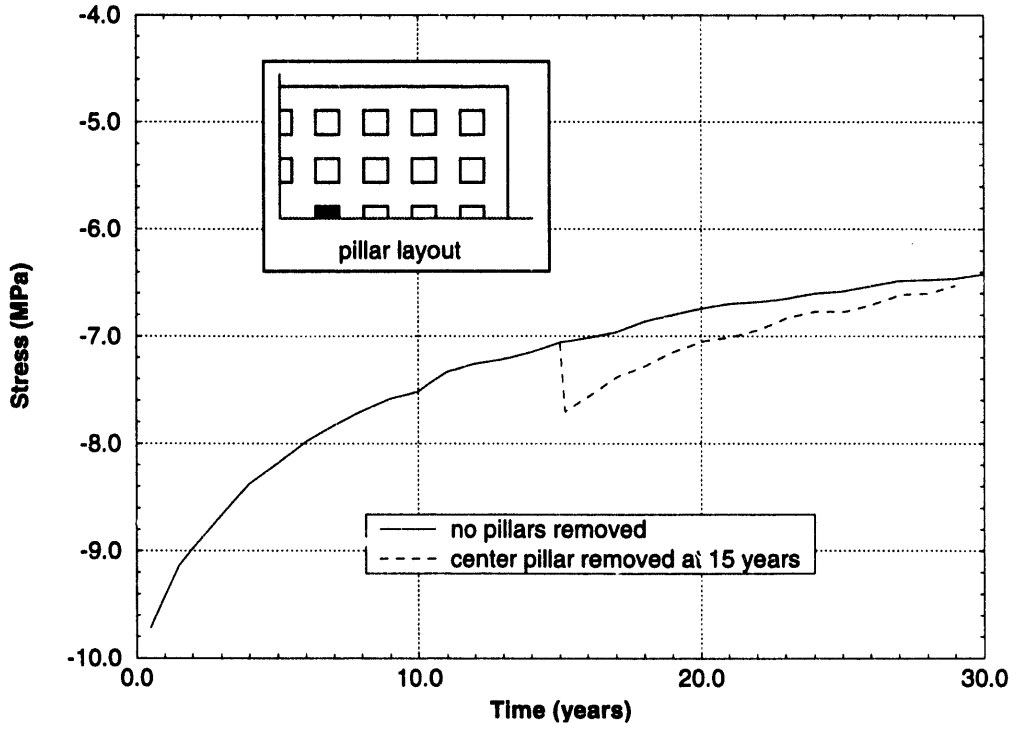

Figure 11. Average vertical stress in neighboring pillar (shown in black) for the cases of (1) center pillar removal and (2) no pillar removal.

expected to decrease in rate. An increasing subsidence rate would indicate progressive failing of the mine. The subsidence and subsidence rate histories are plotted in Figures 12 and 13, respectively, for calculations simulating the loss of 0, 1, 9, 15, 21, and 45 pillars. The calculations simulating the loss of 0, 1, and 45 pillars were performed to 30 years. The calculations simulating the loss of 9, 15 and 21 pillars show only the elastic response to the pillar loss and are therefore not included in the subsidence rate plot. These figures demonstrate that the loss of pillars increases both the amount of instantaneous subsidence due to elastic response and the subsequent subsidence rate due to creep. The rate increases nearly an order of magnitude if all 45 pillars are lost.

A contour plot of the calculated subsidence distribution over the Markel Mine at 30 years is shown in Figure 14 for the case in which no pillars were removed. The mesh lines are shown on the plot to illustrate the extent of subsidence relative to the boundaries of the mine. Also shown in this figure is a vector plot of displacements at 30 years in the same simulation. Both of these figures indicate that ground motion is predominantly vertical above the mine and limited in lateral extent to approximately 150 m from the boundary of the mine. The *angle of draw* is the angle, measured from vertical, of a line drawn from the mine boundary to the subsidence boundary. Based on the results shown in Figure 15, the angle of draw is approximately 45 degrees. Furthermore, the angle of draw does not change significantly with the loss of pillars.

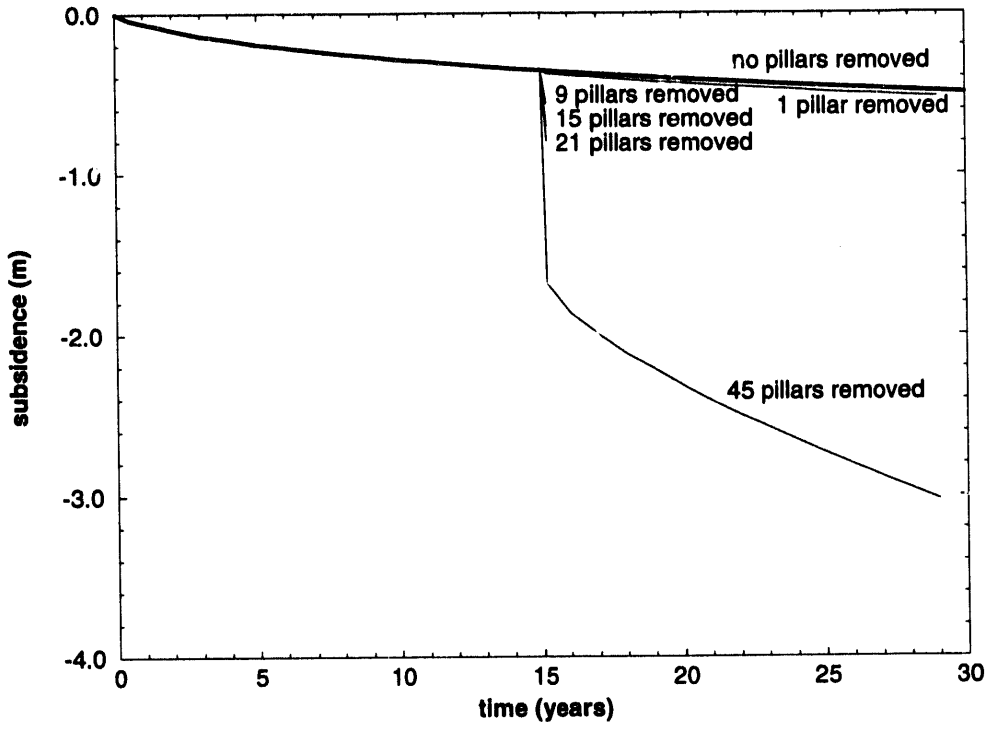

Figure 12. Subsidence history of Markel Mine for the removal of 0, 1, 9, 15, 21, and 45 pillars.

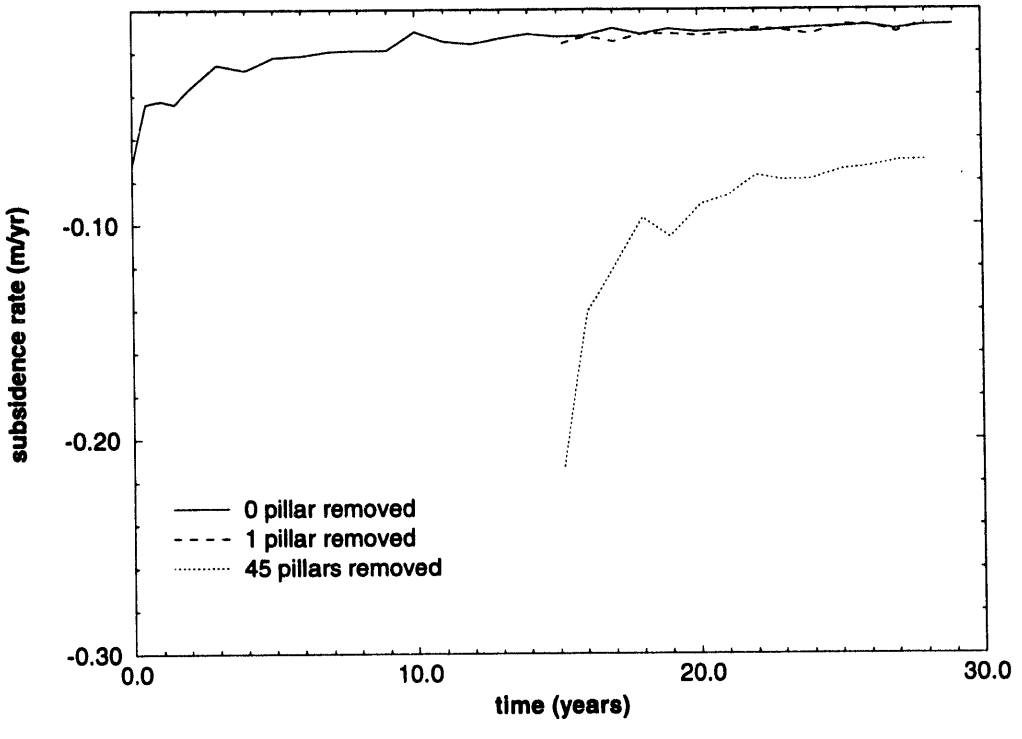

Figure 13. Subsidence rate history of Markel Mine for the removal of 0, 1, and 45 pillars.

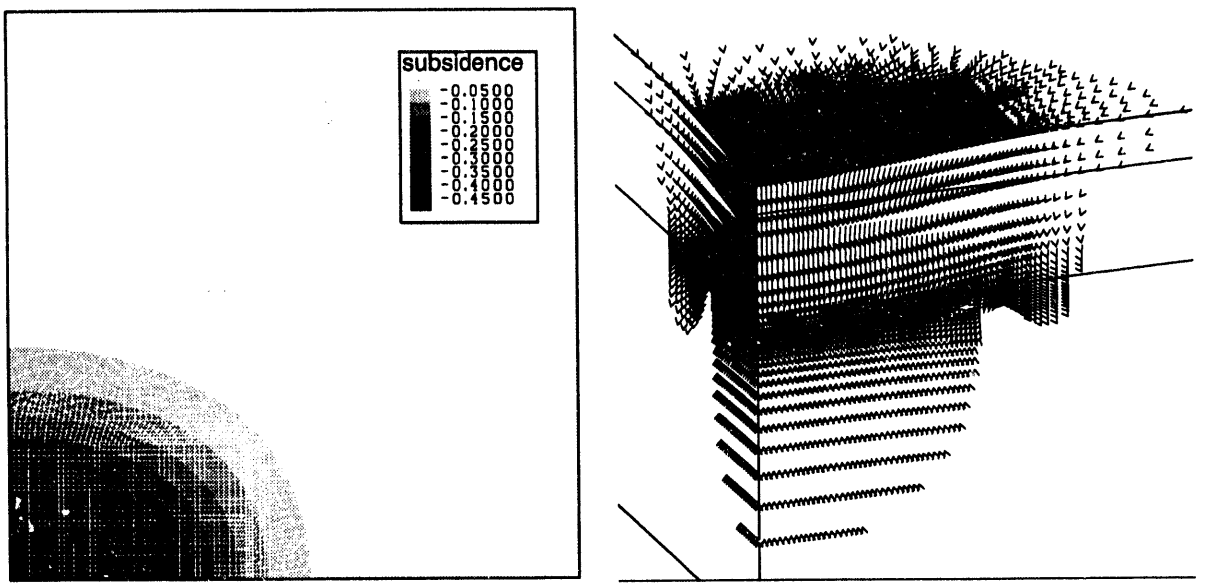

Figure 14. Contour plot of subsidence and vector plot of displacement at 30 years (no pillars removed).

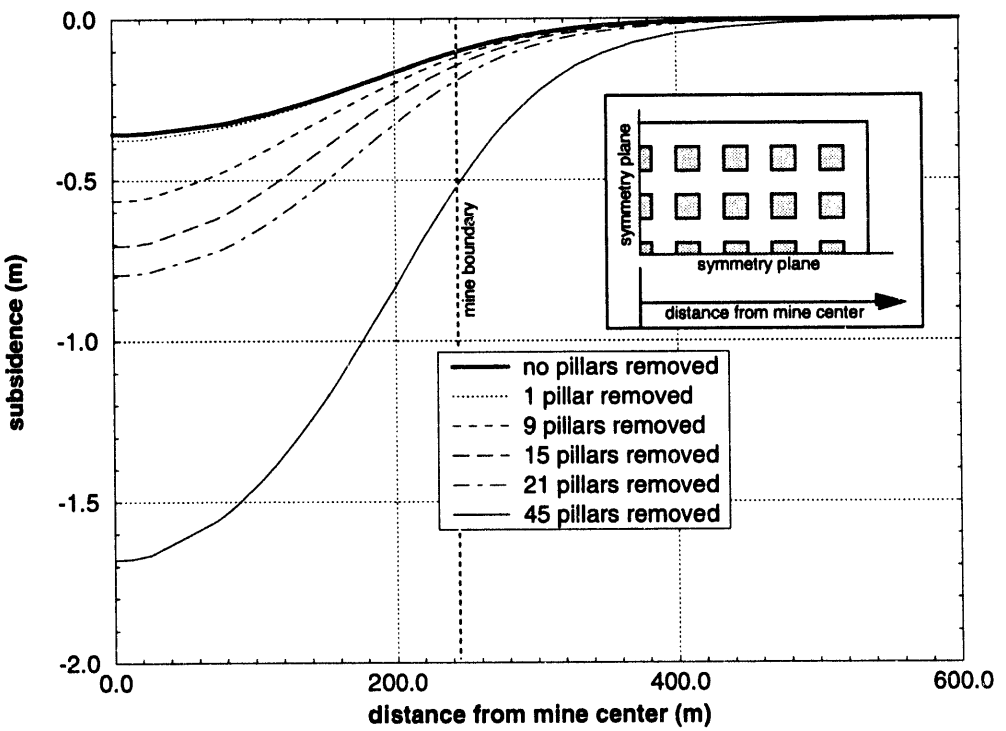

Figure 15. Surface subsidence above the Markel Mine 15 years into the simulation for 0, 1, 9, 15, 21, and 45 pillars removed.

Figure 16 shows a plot of measured subsidence rates [19, 20] over Weeks Island for a group of subsidence stations located in a row as illustrated in the small figure in the top-left corner of the graph. The measured subsidence rates are given for years 1990, 1991, and 1992. The considerable variations in the rates from year to year are probably due to the mining activities in the New Morton Mine. Also shown in the same plot is a profile of the predicted subsidence rate at 15 years into the numerical simulation (corresponding to the 1990 to 1993 time frame). The analysis is mirrored about its plane of symmetry to provide a full subsidence rate profile. The data verifies the prediction that surface subsidence is of limited extent, resulting in a small angle of draw. Since the simulation does not include the New Morton Mine nor the DOE facilities, the predicted subsidence rate is significantly lower than that measured at Weeks Island. Considering the relative size difference between the Markel Mine and the DOE and Morton facilities, the predicted subsidence rate is realistic. Furthermore, if the predicted farfield subsidence rate is adjusted to approximately 0.02 m/yr, equal to the subsidence rate between the Morton and DOE facilities, then the predicted maximum subsidence in the center of the trough is of the same order of magnitude as the measured subsidence rates.

3.3 Pillar Stability

Slabs approximately 3.05 m (10 ft) thick are reported to have fallen from pillars in the benched area of the mine. Acres International Corp. performed several inspections of the Markel Mine [21, 22]. The inspection reports indicate that "the majority of deterioration was on the pillar corners of the 90 ft benched area, with some lesser deterioration occurring along the walls of the 25 ft rooms." The 1990 Acres inspection report [22] indicates that the pillars are developing an hourglass shape as shown in Figure 17, but that this development has a long

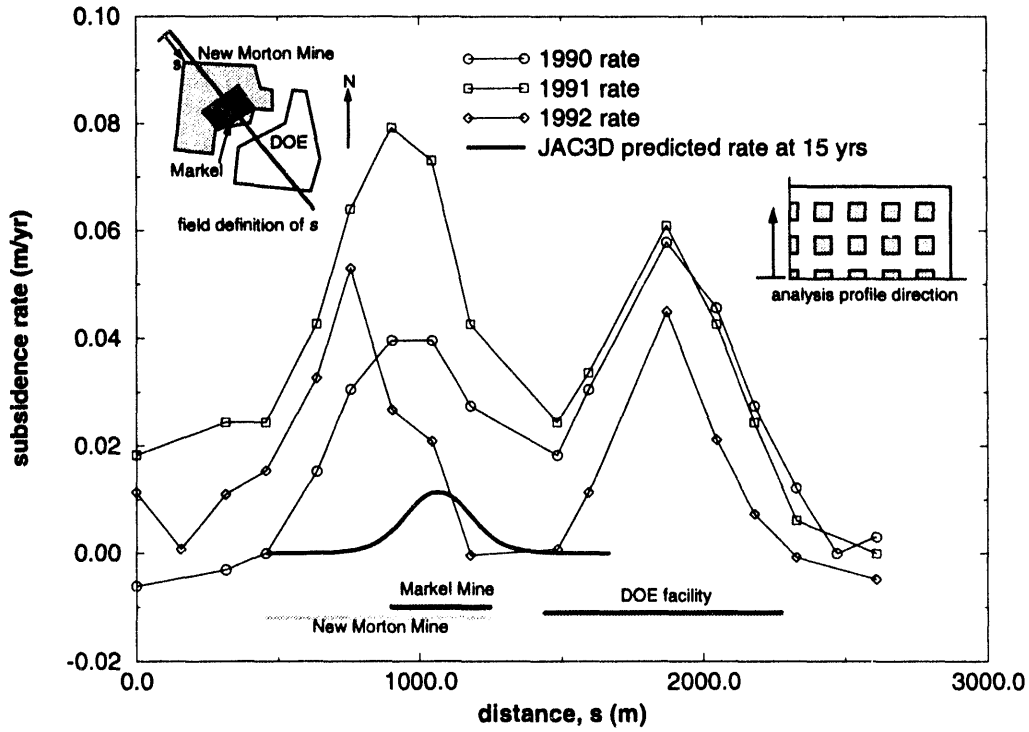

Figure 16. Weeks Island subsidence data [19, 20] compared to the JAC3D predicted subsidence profile at 15 years. Approximate survey line shown in figure.

way to go before the hourglass shape is fully achieved. Furthermore, this report indicates that the number of large salt falls observed was decreasing in time with a proportional increase in the small falls observed. The 1989 Acres inspection report indicates that there has been little or no change in the condition of the mine in the previous three years [21]. Hence, it is reasonable to assume that the majority of the large salt falls occurred within the first five years after Markel mining operations ceased.

3.3.1 Tensile Failure

A plot of the calculated maximum principal stress distribution in the Markel Mine 2 years after formation is shown in Figure 18. These regions of tensile stress correspond to failures observed in the roof and walls of the Markel Mine. The tensile regions in the walls are approximately 3 m (10 ft) thick at mid-height. Note that the tensile regions develop in the walls of the benched area and not the unbenched area. This is consistent with the inspection reports which indicate that the majority of deterioration occurred in the benched area. The predicted tensile stresses develop upon excavation of the mine and increase in magnitude during the first three to four years to a maximum of approximately 1.25 MPa. The time frame of predicted tensile stress growth (three to four years) agrees with the time period during which the largest salt falls were observed. Furthermore, if the material in tension is removed, the pillar assumes an hourglass shape as observed in the mine. Figure 19 is a vector plot showing the orientation of the tensile stresses in a pillar at 2 years. The tensile stresses are oriented parallel to the wall surface. Cracks resulting from these tensile stresses should generally be vertical and perpendicular to the face of the pillar. The majority of cracks

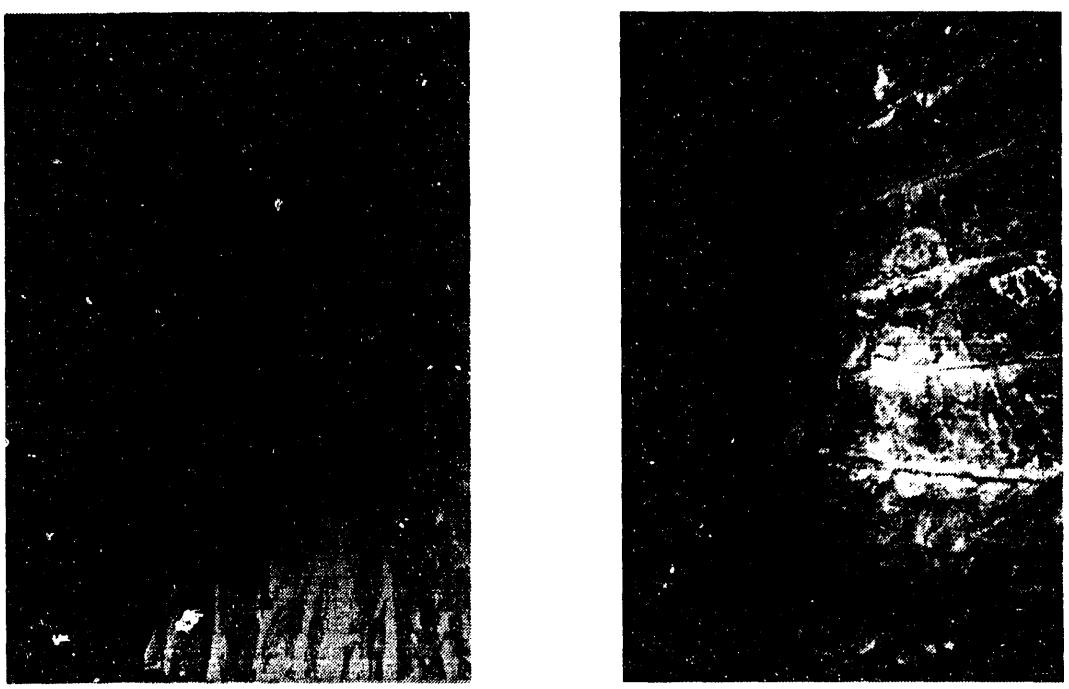

Figure 17. Slabbing of the Markel Mine pillars, resulting in a post-failure hourglass shape (1989) [21].

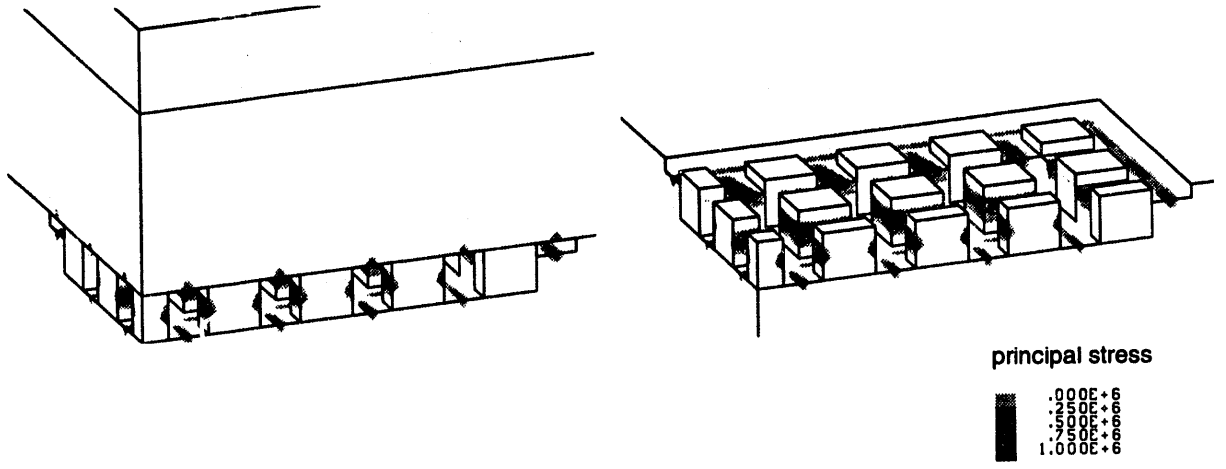

Figure 18. Plot of maximum principal stress distribution in Markel Mine at 2 years.

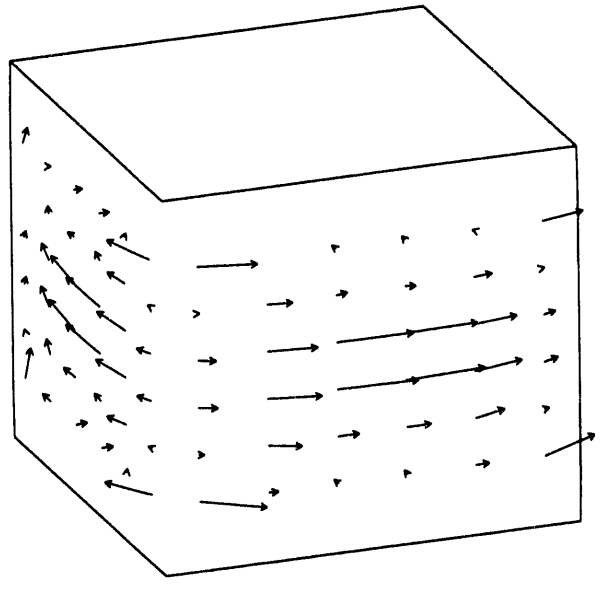

Figure 19. Orientation of tensile principal stresses in the Markel Mine pillars.

observed in the Markel are vertical. Corner slabbing could be caused by the intersection of tensile cracks originating from orthogonal faces as shown in Figure 20.

A slabbing pillar model of the Markel Mine, shown in Figure 21, was developed to determine how the stress distribution in the pillars is affected by slabbing. The center-most 21 pillars (benched area) are meshed such that a 3.05 m (10 ft) thick slab of salt can be removed from all four walls of the pillar, yielding an hourglass pillar shape. It should be noted that all of the computational results from this model represent a worst case in which all of the pillars in the benched area slab on all four sides at the same time. The slabbing observed in the Markel Mine has occurred more gradually and is not as complete.

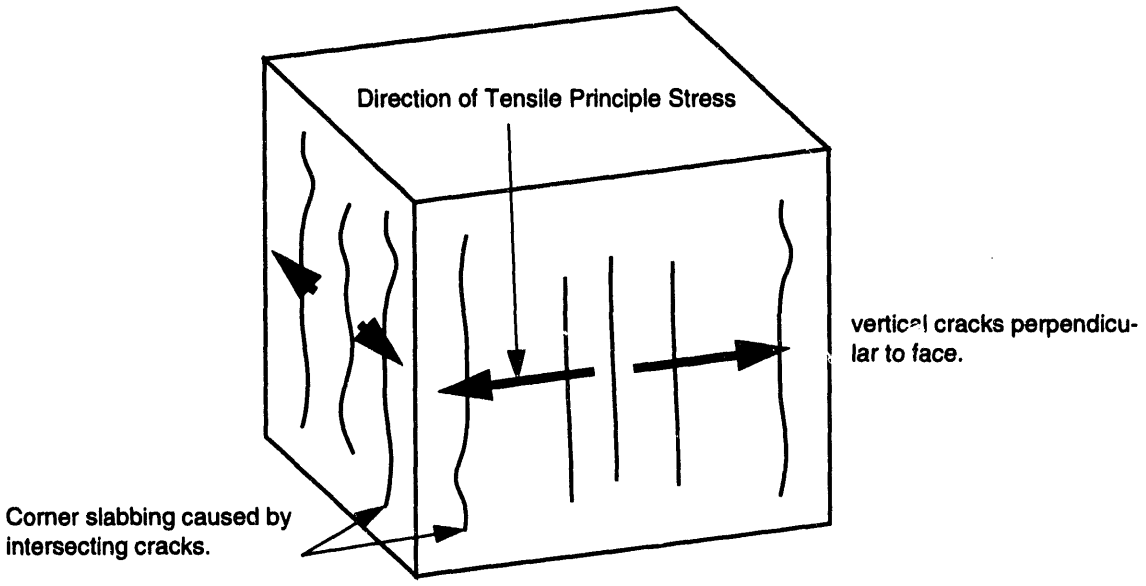

Figure 20. Proposed crack orientations due to tensile principal stresses in the pillar.

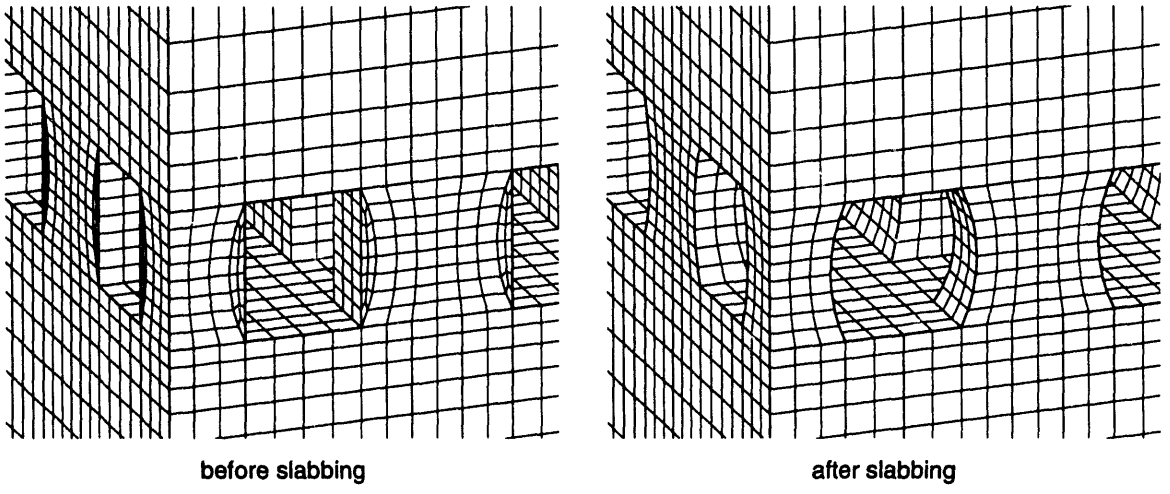

Figure 21. Slabbing pillar model of the Markel Mine.

As previously noted, the observed large salt falls in the Markel Mine took place in the first few years of operation [23]. To be consistent with this observation, a 20-year simulation was performed in which the slab material was deleted two years into the simulation. Figure 22 shows a contour plot of maximum principal stress in the center-most pillar at three times in the analysis: (a) prior to slabbing, (b) immediately after slabbing, and (c) at the end of the 20 year simulation. Prior to slabbing (2 years), a region of tensile stress develops which is approximately 3.05 m (10 ft) thick at the pillar mid-height. After this region of material is removed, the stress distribution in the pillar changes such that there are no tensile stresses in the pillar. The stress distribution changes because the hourglass shape places the pillar in confinement. Twenty years into the simulation (18 years after slabbing) the maximum principal stresses in the pillars remain compressive. Hence, the analysis results suggest that corner slabbing is initiated early in the life of the mine by the development of tensile stress in the pillar. The post-slabbing shape of the pillar results in the redistribution of stresses such

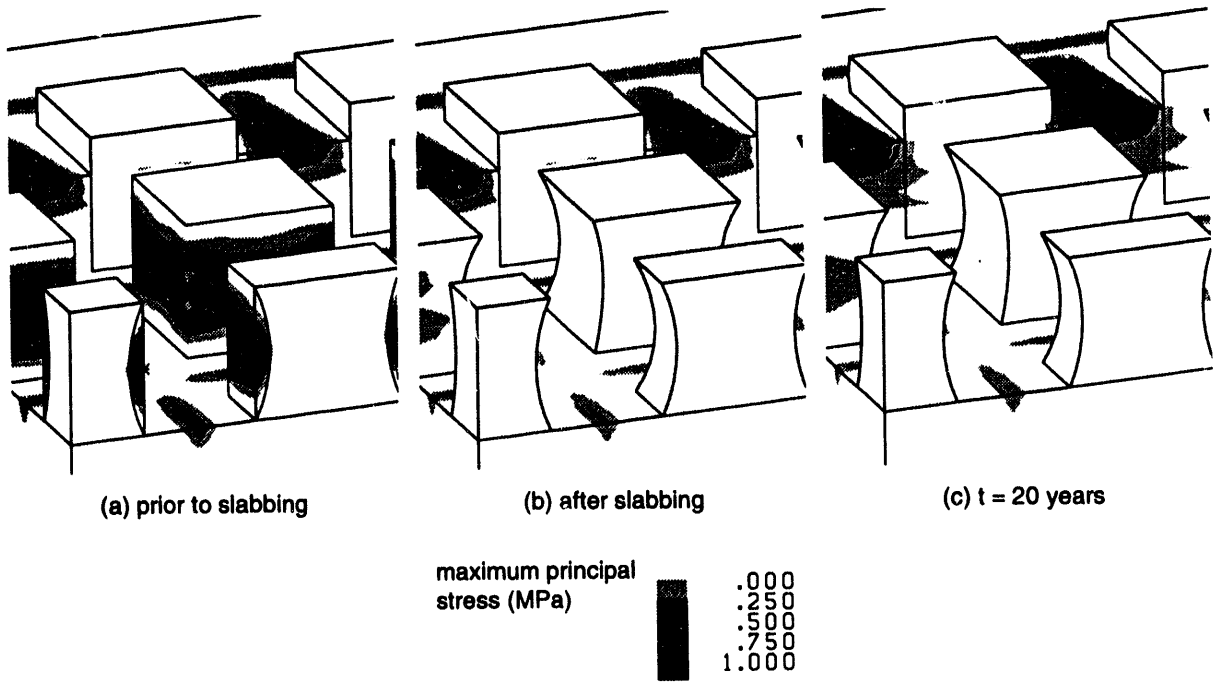

Figure 22. Contour plot of maximum principal stress in the pillars of the Markel Mine (a) prior to slabbing, (b) immediately after slabbing, and (c) at the end of the 30 year simulation.

that no further failure will occur as a result of tensile stress, indicating that the mine is stable with respect to this failure mechanism.

It is interesting to note that the high tensile regions predicted at the edge of the unbenched area correspond with the location of fractures observed in the floor of the Markel Mine. These fractures are known as *floor heave* [21]. Although floor heave has no apparent effect on mine stability, this agreement provides further confidence in the computational results.

Based on the above comparisons between the analysis and field observations, it is proposed that the corner slabbing observed in the Markel Mine is probably due to the development of tensile stresses in the pillars as opposed to creep rupture. This assumption is supported by the fact that there has been a decreasing number of large salt falls since these early failures [23]. Conversely, creep rupture is a progressive failure mode. Hence, one would expect failure by this mechanism to increase as creep strains in the pillar increased.

3.3.2 Compressive Failure

Another concern is that slabbing reduces the load bearing area of the pillar, reducing the factor of safety originally designed into the pillars. Three additional factors should be considered: (1) the load bearing area of the pillar is increasing as the pillar bulges due to creep, (2) the load applied to the pillar is decreasing in time as seen in Figures 6 and 11, and (3) the post-failure hourglass shape increases the confining pressure in the pillar which increases the limits of both instantaneous (Mohr-Coulomb) failure mechanisms as well as time dependent (creep rupture) failure mechanisms. Figure 23 shows the pressure distribution in the center pillar before and after slabbing. The minimum confining pressure before

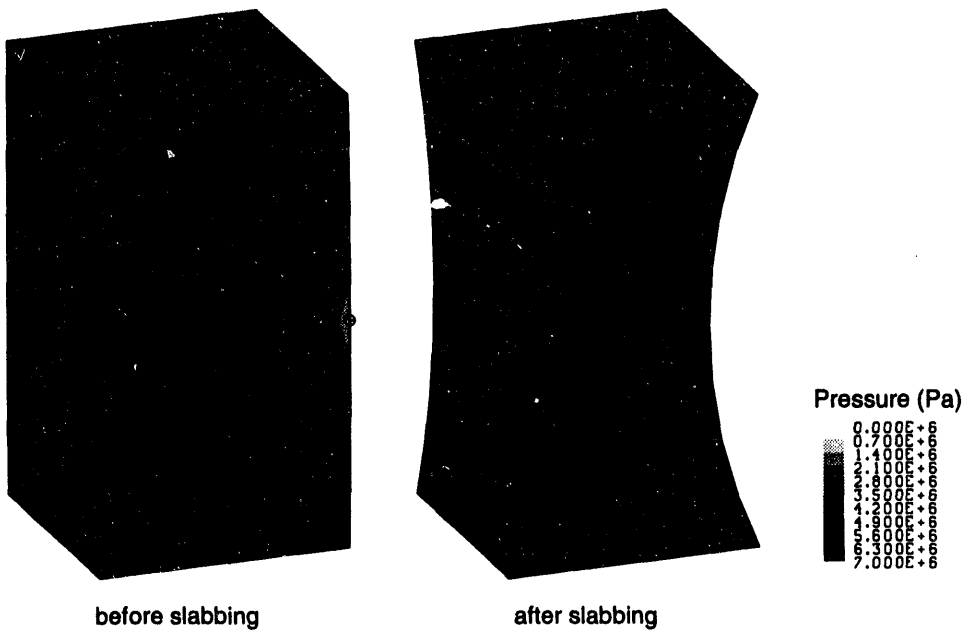

Figure 23. Pressure distribution in the center before and after slabbing.

slabbing is approximately 2 MPa (290 psi). After slabbing, the minimum confining pressure increases to 4 MPa (580 psi). The compressive strength of salt increases from approximately 13.8 MPa (2000 psi) for no confining pressure to approximately 52 MPa (7600 psi) for 3.4 MPa (500 psi) confining pressure [8]. The elastic stability function presented in Table 2 is plotted in Figure 24 for the center pillar before and after slabbing. In this plot the octahedral stress is normalized with respect to the octahedral strength (τ_{0B}). Thus, elastic instability is indicated in regions where $F \leq 1.0$. Before slabbing, the minimum value of the elastic stability function is 1.08. After slabbing the minimum value increases to 1.35. Even 18 years after slabbing, the minimum value of the elastic stability function increases further to 1.55. Thus, slabbing improves the condition of the pillar with respect to elastic stability. This occurs because the increased confinement resulting from the hourglass geometry compensates for the reduction in load bearing area.

The vertical stress distribution in the center pillar before and after slabbing is shown in Figure 25. The maximum stress in the pillar increases from 11 MPa to 13.7 MPa (25 percent). The average vertical stress in the core of the pillar (the portion which remains after slabbing) is plotted in Figure 26 as a function of time. The average stress increases from 9.46 MPa prior to slabbing to 12 MPa after slabbing (a 27 percent increase). However, because the average stress in the pillar is decreasing with time, this is only 17 percent higher than the original pillar stress of 10.2 MPa and still below the 13.9 MPa unconfined compressive strength of rock salt. Furthermore, the average stress reduces back to its original (t=0) value only 2.5 years after slabbing. Thus, the period of inactivity reported in the 1989 inspection report would be sufficient for the average vertical stress in the pillar to reduce such that future compressive failure is unlikely unless slabbing continues to reduce the cross sectional area of the pillar.

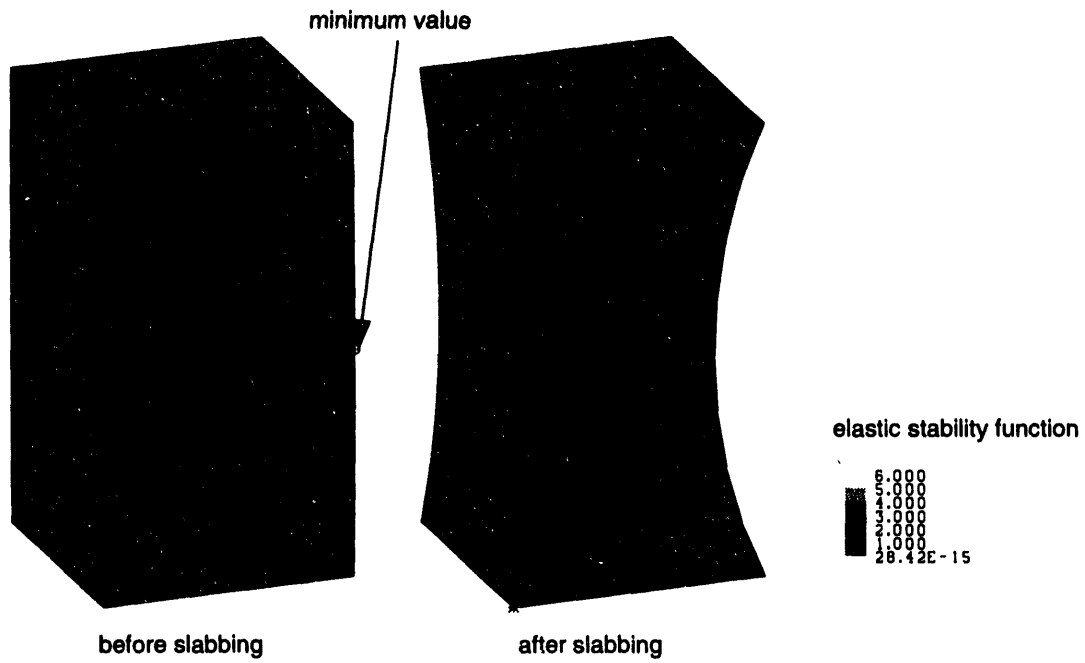

Figure 24. Elastic stability function plotted for the center pillar before and after slabbing.

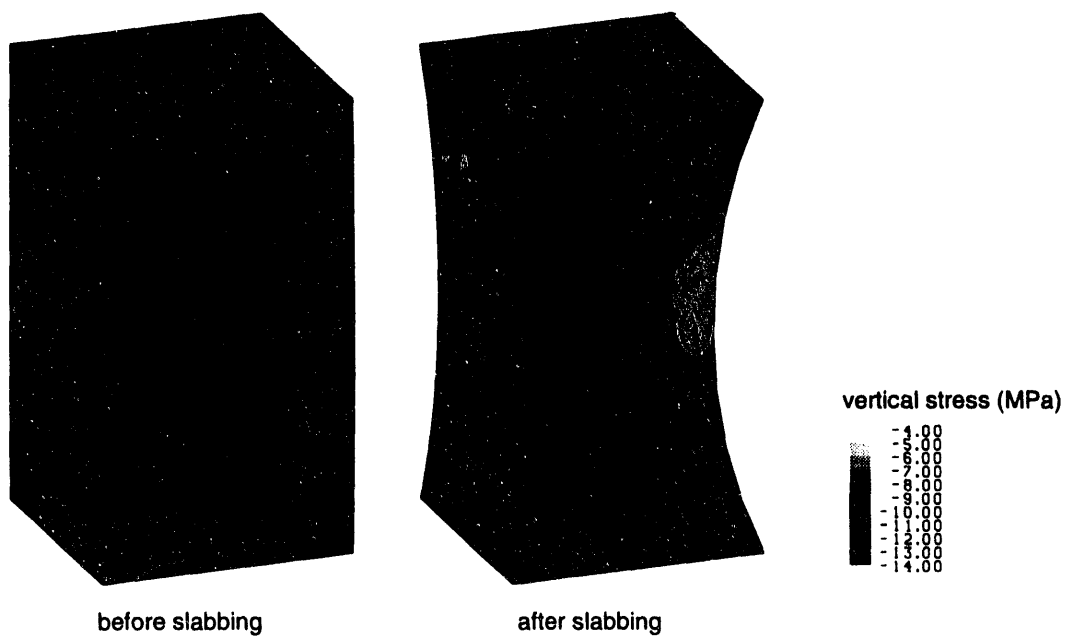

Figure 25. Vertical stress distribution in the center pillar before and after slabbing.

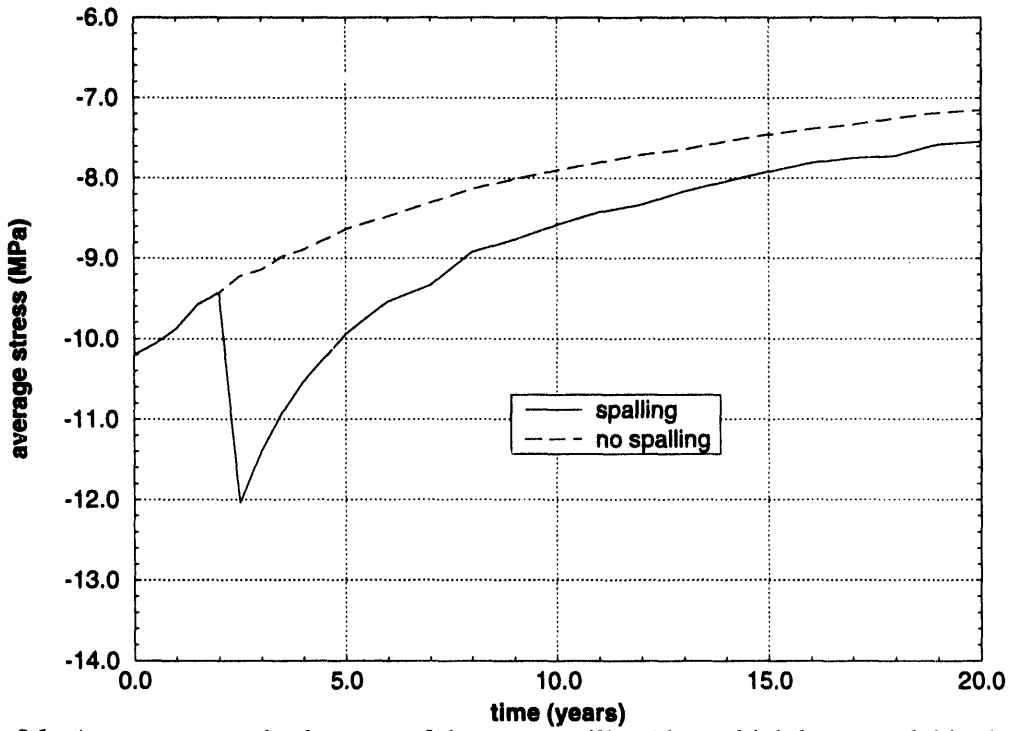

Figure 26. Average stress in the core of the center pillar (that which has not slabbed) as a function of time.

3.3.3 Creep Rupture

Creep rupture is the least understood of the three failure mechanisms considered here for rock salt. The criterion used in this analysis is based on a limiting strain derived from quasistatic laboratory test data. Although the criterion has not been extensively validated against field data, it is the best available measure of the creep rupture performance of Weeks Island salt. A contour plot of the failure criterion is presented in Figure 27 at 3 years and 17 years in the simulation. Seventeen years corresponds to the approximate age of the mine at present. Failure is indicated by regions in which the failure function is less than one. Failure initiates approximately three years into the simulation and starts in the center-most pillars. The failure initiates from the outer walls of the pillar at mid-height. The failure region gradually moves toward the center of the pillar. The criterion indicates that, at present (17 years into the simulation), through-pillar failure has occurred from top to bottom of all the pillars in the benched area. Since this is a strain-limiting criterion, the shapes of the failure contours are similar to those of creep strain (see Figure 5). It is difficult to confirm creep rupture based on visual inspection of a pillar since failure by this mechanism can be manifested in intergranular fracturing coupled with a loss in pillar strength but with no visible signs of deterioration. Creep rupture may be the cause of some of the failure attributed to tensile fracture. Even if this criterion is conservative, predicting failure to occur too soon, the shape of the failed region should be as predicted if creep rupture is strain based as is commonly believed. If, as predicted by this strain limiting criterion, the pillars are failing, then the present state of the mine would be equivalent to removing the center 21 pillars (see Figure 8). The additional load placed on the unbenched pillars would eventually cause them to fail, resulting in the loss of

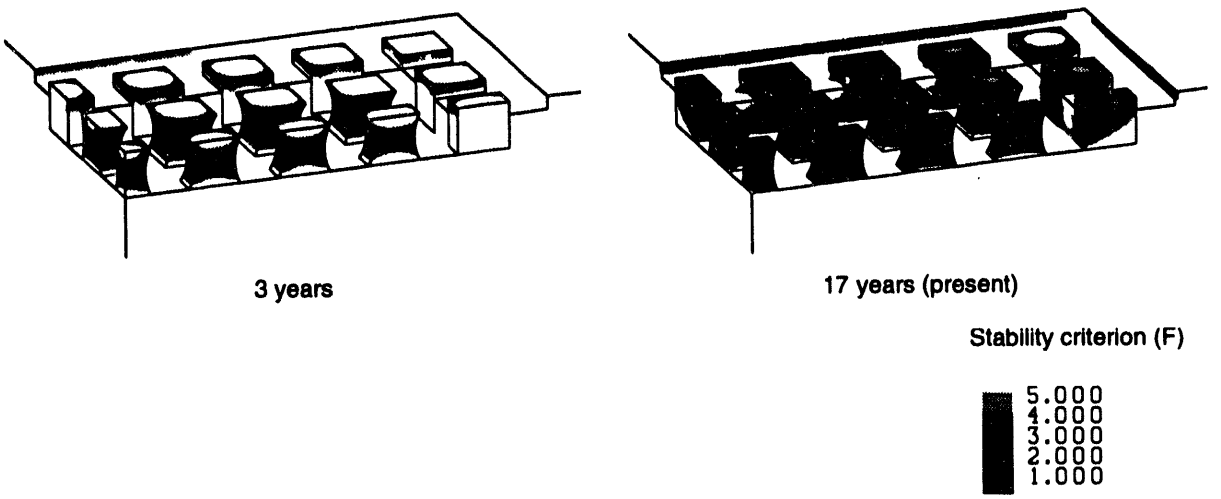

Figure 27. Creep rupture criteria plotted at 3 years and 17 years (present). Failure is indicated in regions where $F < 1$.

strength in all 45 pillars. As was shown in Section 3.2, the loss of all pillars will result in the development of tensile stress s from the mine to the salt/overburden interface and possibly create a path for water to enter the mine.

4 Discussion and Conclusions

A three dimensional finite element analysis of the Markel Mine located on Weeks Island was performed to: (1) evaluate the stability of the mine and (2) determine what effects mine failure might have on the nearby Morton Salt mine and SPR facilities. The simulations performed with this finite room and pillar model of the Markel Mine revealed performance characteristics of the mine which could not be determined from previously used infinite room and pillar models. First, subsidence due to creep closure is localized over the Markel Mine with the maximum subsidence occurring over the center of the mine. This behavior is consistent with subsidence data from the Weeks Island site. Second, the stress in the pillars of the Markel Mine is reducing with respect to time. This stress reduction is the result of (1) an increase in the load bearing area of the pillar as it bulges, and (2) a reduction in the load applied to the pillar, implying that the pillars are creeping faster than the mine roof. The later performance characteristic has an significant impact on the stability of the mine, demonstrating that this model is more appropriate for investigating stability issues than an infinite room and pillar model.

The stability investigation consisted of two studies. The first part of the stability evaluation investigates the effect of pillar failure on the integrity of the overlying salt and overburden. Based on a study in which selected pillars were removed from the model to simulate pillar failure, the following observations are presented:

- *The loss of a single pillar in the Markel Mine will not cause the failure of its surrounding pillars.* The loss of one pillar results in a 10 percent increase in the average stress in the neighboring pillars. Because the stress in the pillars is reducing in time, this increase results in a stress significantly less than the original elastic pillar stress (at time t=0).
- *Ground water intrusion is possible if some the Markel Mine pillars fail.* Tensile stresses start to develop in the overburden with the loss of only 1 pillar. These tensile stresses extend from the mine to the salt/overburden interface only for the case where all pillars are removed simultaneously. These tensile stresses could cause macroscopic fracturing of the salt and result in the development of a path for water to enter the mine. A disturbed rock zone (DRZ) or dilatant region develops as pillars are removed from the model. The DRZ bridges the mine and the overburden in the case where 15 or more pillars are removed from the model. Dilatant damage is attributed to microfracturing or changes in the pore structure of the salt, resulting in a flow path for groundwater to enter the mine.
- *Complete collapse of the Markel Mine could cause damage to the service shaft of the New Morton Mine.* The tensile stresses resulting from the loss of all pillars extend approximately 213 m (700 ft) from the boundary of the Markel Mine. This poses a threat to the service shaft of the New Morton Mine as it is only 152 m (500 ft) away from the Markel Mine. The tensile stresses could cause the Morton Mine service shaft to separate from its host salt and possibly create a flow path behind the shaft lining. Indirectly, the service and production shafts of the New Morton Mine could also be threatened by flooding of the Markel Mine as only 18 m (60 ft) of salt separates the shafts from an access drift of the Markel.

In the second part of the stability evaluation, the stability of the pillars is investigated with respect to three failure mechanisms: tensile failure, compressive failure, and creep rupture. A slabbing pillar model was developed to investigate how the failures observed in the Markel Mine affect the stress distribution in the pillar. Although the model simulates slabbing of a greater extent than that observed in the Markel Mine, the results are indicative of the stress redistributions that the pillars are undergoing. With respect to the three failure criteria, the following observations are presented:

- *Tensile failure.* The timing of the corner slabbing observed in the Markel Mine (occurring in the first three to four years) agrees with the predicted development of tensile stresses in the pillar walls. Furthermore, if the material in tension is removed, the pillars assume an hourglass shape as observed in the Markel Mine. Numerical simulations reveal that the stresses in the post-slabbed hourglass shape redistribute such that there are no tensile stresses. Thus, failure due to this criterion is not likely to occur after the hourglass shape is fully achieved.
- *Compressive failure.* The average vertical stress increases 27 percent due to the reduced cross sectional area of the pillar after slabbing has occurred. However, because the applied load is decreasing with time, the average vertical stress reduces to its original value in less than 3 years. Furthermore, the post-failure hourglass pillar shape results in increased confinement. Higher confinement stresses result in an increase in the yield strength of rock salt. Finally, after slabbing has occurred, the cross sectional area of the pillar is increasing with time as it bulges. Thus, failure due to exceeding the compressive strength of salt is not likely unless the cross sectional area of the pillar is further reduced.
- *Creep Rupture.* Based on the criterion used in this evaluation, failure by this mechanism is predicted to begin approximately three years into the life of the mine. At present, through-pillar failure is predicted to occur in all of the pillars in the benched area. It is uncertain how much of the observed slabbing, if any, has been caused by creep rupture. It is possible that the failure observed up to now has been a combination of tensile failure and creep rupture. If, according to the criterion used in this evaluation, the pillars are failing by this mechanism, then the accompanying loss of strength would be equivalent to removing pillars from the model as was done in the first part of this stability analysis. Since the pillars in the benched area are at the same extent of creep rupture, then the present state of the mine would be equivalent to the case in which the center-most 21 pillars are removed. The additional load placed on the unbenched pillars would eventually cause them to fail, resulting in the loss of strength in all 45 pillars.

Of the various failure criteria investigated, the most alarming results are predicted by the creep rupture criterion. Since creep rupture is not a well understood phenomena and the present criterion is not sufficiently validated against laboratory and field data, further development and validation of failure criteria is recommended.

5 References

1 Acres International Corporation, "Weeks Island Strategic Petroleum Reserve Geological Site Characterization Report," SAND87-7111, June 1987.

2 J. H. Biffle, "JAC3D - A Three-Dimensional Finite Element Computer Program for the Nonlinear Quasistatic Response of Solids with the Conjugate Gradient Method," SAND87-1305, Sandia National Laboratories, Albuquerque, New Mexico; In Preparation.

3 E. L. Hoffman, "Investigation of Analysis Assumptions for SPR Calculations," memo to J. K. Linn, Sandia National Laboratories, Albuquerque, New Mexico, February 7, 1992.

4 R. D. Krieg, "Reference Stratigraphy and Rock Properties for the Waste Isolation Pilot Plant (WIPP) Project," SAND83-1908, Sandia National Laboratories, Albuquerque, New Mexico, January 1984.

5 W. Herrmann and H. S. Lauson, "Analysis of Creep Data for Various Natural Rock Salts," SAND81-2567, Sandia National Laboratories, Albuquerque, New Mexico, December 1981.

6 W. Herrmann and H. S. Lauson, "Review and Comparison of Transient Creep Laws Used for Natural Rock Salt," SAND81-0738, Sandia National Laboratories, Albuquerque, New Mexico, April 1981.

7 U. Hunsche and H. Albrecht, "Results of True Triaxial Strength Tests on Rock Salt," *Engineering Fracture Mechanics*, Vol 35, No. 4/5, pp. 867-877, 1990.

8 Acres American Inc., "U. S. Federal Energy Administration National Strategic Oil Storage Program; Weeks Island Mine Geotechnical Study," November 1977.

9 R. E. Goodman, "Introduction to Rock Mechanics," John Wiley & Sons, New York, 1980.

10 B. L. Ehgartner, "Weeks Island Creep Failure Criteria," memo to distribution, Sandia National Laboratories, April 20, 1993.

11 J. C. Stormont, C. L. Howard, and J. K. Daemen, "Changes in Rock Salt Permeability due to Nearby Excavation," Rock Mechanics as a Multidisciplanary Science Proceedings of the 32nd U. S. Symposium, 1991.

12 L. L. Van Sambeek, J. L. Ratigan, and F. D. Hansen, "Dilatancy of Rock Salt in Laboratory Tests," The 34th U. S. Symposium on Rock Mechanics, 1993.

13 U. E. Hunsche, "Failure Behaviour of Rock Salt Around Underground Cavities," 7th International Symposium on Salt, 1992.

14 C. J. Speirs, C. J. Peach, R.H. Brzesowsky, P.M.T.M. Schutjens, J. L. Liezenberg, and H.J. Zwart, "Long Term Rheological and Transport Properties of Dry and Wet Rocks, EUR 11848, prepared for Commission of the European Communities, by University of Utrecht, Utrecht, The Netherlands, 1988.

15 J. L. Ratigan, L.L. Van Sambeek, K.L. De Vries, and J.D. Nieland, "The Influence of Seal Design on the Development of the Disturbed Rock Zone in the WIPP Alcove Seal Tests," Topical Report RSI-0400, prepared by Parsons Brinkerhoff, San Francisco, CA, and RE/SPEC Inc., Rapid City, SD, for Sandia National Laboratories, Albuquerque, NM, 1991.

16 B. L. Ehgartner, "Dilatancy Criterion for Weeks Island Salt," memo to J. K. Linn, Sandia National Laboratories, Albuquerque, NM, February 21, 1994.

17 W. R. Wawersik, D. W. Hannum, H. S. Lauson, "Compression and Extension Data for Dome Salt from West Hackberry, Louisiana," SAND79-0668, Sandia National Laboratories, Albuquerque, NM, 1979.

18 B. L. Ehgartner, "Simulation of Markel Mine Collapse," memo to J. K. Linn, Sandia National Laboratories, Albuquerque, NM, May 5, 1993.

19 Boeing Petroleum Services, Inc., "SPR Annual Subsidence Report," Pub. no. D506-03165-09, Oct. 19, 1992.

20 J. T. Jakubik, "Dec 92 Survey of Weeks Island," letter to Boeing Petroleum Services, Dec. 15, 1992.

21 Acres International Corporation, "Report on Markel Mine Inspection," March 1989.

22 Acres International Corporation, "Report on Markel Mine Inspection," March 1990.

23 Private discussion with James Neal, participant in past inspections of the Markel Mine.

Distribution

US DOE SPR PMO (5)
900 Commerce Road East
New Orleans, LA 70123
Attn: J. Culbert, FE 4431
J. C. Kilroy, FE 433
J. W. Kunkel, FE 4422
R. E. Meyers, FE 4422
L. Rousseau, FE-433

US Department of Energy (3)
Strategic Petroleum Reserve
1000 Independence Avenue SW
Washington, DC 20585
Attn: D. Johnson, FE 421
D. Smith, FE 423
D. Buck, FE 421

DynMcDermott Petroleum Operations
850 S. Clearview Parkway
New Orleans, LA 70123
Attn: K. Mills

Weeks Island SPR Site (2)
P.O. Box 434
New Iberia, LA 70560
Attn: M. Jackson
R. Phillips

RE/SPEC, Inc.
3824 Jet Drive
Rapid City, SD 57709
Attn: J. L. Ratigan

Sandia internal:

MS0439	1434	D. R. Martinez
MS0841	1500	D. J. McCloskey
MS0836	1501	C. W. Peterson Route to: 1512, 1513, 1551, 1552
MS0827	1502	P. J. Hommert Route to: 1503, 1511, 1553, 1554
MS0441	1503	J. H. Biffle
MS0443	1561	H. S. Morgan
MS0443	1561	M. L. Blanford
MS0443	1561	E. L. Hoffman (6)
MS0443	1561	J. G. Arguello
MS0443	1561	C. M. Stone
MS0443	1561	J. R. Weatherby
MS0437	1562	R. K. Thomas
MS0701	6100	R. W. Lynch
MS0706	6112	D. A. Northrop
MS0706	6113	S. J. Bauer
MS0706	6113	B. L. Ehgartner (5)
MS0706	6113	T. E. Hinkebein
MS0706	6113	P. S. Kuhlman
MS0706	6113	J. K. Linn
MS0706	6113	M. A. Molecke
MS0706	6113	J. T. Neal
MS0706	6113	R. W. Ostensen
MS0706	6113	J. L. Todd
MS0706	6113	S. T. Wallace
MS0750	6116	D. J. Borns
MS0751	6117	W. R. Wawersik
MS0751	6117	D. H. Zeuch
MS0751	6117	D. S. Preece
MS1322	6121	F. D. Hansen
MS1322	6121	D. E. Munson
MS1322	6121	J. R. Tillerson
MS0899	7141	Technical Library (5)
MS0619	7151	Technical Publications
MS0100	7613-2	Document Processing for DOE/OSTI (10)
MS9018	8523-2	Central Technical Files

DATE
FILMED
8/29/94
END